THE ASTROPHYSICAL JOURNAL SUPPLEMENT SERIES, 105:353–368, 1996 August

THE DISTRIBUTION AND PROPERTIES OF H II REGIONS IN EARLY-TO-INTERMEDIATE HUBBLE TYPE RINGED GALAXIES

DEBORAH A. CROCKER,[1] PAMELA D. BAUGUS,[2] AND R. BUTA[1]
Received 1995 September 6; accepted 1995 December 5

ABSTRACT

This paper presents a study of the H II regions in 32 ringed and pseudoringed galaxies having Hubble types in the range $S0^+$ to Sc. The objective is to illustrate the distributions of H II regions in classic examples of ringed galaxies and to relate the observed properties to resonance theory. The sample is selected from the Catalog of Southern Ringed Galaxies and includes examples covering a range of ring and galaxy morphological properties. We find that the distribution of Hα luminosity around inner rings is sensitive to the intrinsic shape of the rings. Extremely oval inner rings show a greater concentration of H II regions near the intrinsic ring major axis compared to more circular rings. Nuclear rings are present in several of the sample galaxies and show a range of morphological properties, from a double nuclear ring in NGC 1317 to an irregular feature in NGC 1433. We find also that in galaxies in which an R_1 outer ring is prominent in the continuum image, the H II regions follow an R'_2 morphology. In several cases, the observed distribution of H II regions strongly supports the idea that the rings are linked to specific orbital resonances with the bar.

H II region luminosity functions have been derived for all of the sample galaxies. The functions can be represented by power laws whose exponents are very similar to those found for nonringed galaxies. In a few cases, a luminous nuclear ring produces a secondary peak in the luminosity function. One galaxy shows a break in the luminosity function similar to that observed in other galaxies by Kennicutt, Edgar, & Hodge.

The most unusual Hα distribution in the sample was found in the large outer-ringed galaxy NGC 1291. The primary bar, lens, and secondary bar regions of this S0/a galaxy are filled with a wispy pattern of ionized gas filaments very reminiscent of what is seen in the bulge of M31.

Subject headings: atlases — galaxies: ISM — galaxies: spiral — galaxies: structure — H II regions

1. INTRODUCTION

The properties and distribution of H II regions in a disk galaxy contain information on star formation, internal dynamics, and conditions in the interstellar medium. In late-type galaxies such as irregulars, H II regions are distributed in a clumpy, asymmetric manner, and their properties may be tied mainly to local effects (Gallagher & Hunter 1984). In early-type galaxies, H II regions tend to be considerably less luminous than in irregulars of the same absolute magnitude (Kennicutt 1988, hereafter K88) and appear associated mainly with spiral structure. Of particular interest is how in some early-type galaxies, recent star formation is confined entirely or mostly to ring-shaped zones, as indicated in color index maps or Hα images. Excellent examples are NGC 3081, 7020, 7187, 7702, and others illustrated by Buta & Crocker (1991), Pogge & Eskridge (1993), and in the Catalog of Southern Ringed Galaxies (Buta 1995, hereafter CSRG). In these cases, the star formation is almost certainly tied to internal dynamics, the most promising interpretation being that the rings are caused by the gathering and subsequent compression of gas near orbital resonances with a bar, oval, or spiral density wave perturbation.

Little is known about star formation rates and H II region luminosity functions in classic ringed galaxies such as the above examples. Since ringed galaxies are not rare and represent fairly simple disk galaxies to interpret dynamically (because the positions and morphologies of rings can be tied to internal dynamics more easily than the features seen in pure spirals, for example), it is interesting to examine the star formation in rings of various subtypes. Papers by K88, Kennicutt, Edgar, & Hodge (1989, hereafter KEH), and Caldwell et al. (1991) have been concerned with H II regions in normal galaxies (not necessarily ringed) and have highlighted what can be learned from H II region sizes, luminosities, luminosity functions, and distributions. One of our principal goals in this paper is to determine whether the distribution of H II regions in a ring is sensitive to the intrinsic shape of the ring and its orientation with respect to the bar. Near resonance regions, the gas can be gathered into periodic orbits that are distinctive. If stars form in the gas, the shape of the resulting ring can resemble the shape and orientation of a major family of periodic orbits. We expect the distribution of H II regions to be sensitive to the properties of these orbits. For example, if a ring lies close to but inside corotation (as is believed to be the case for inner rings), gas will spend more time near the major axis of the ring than the minor axis (Contopoulos 1979). Thus, near the true major axis of an elongated inner ring, we expect H II regions to "bunch" up. Outer rings are associated with different families of periodic orbits, and we expect to see also some of these differences in the distribution of star formation.

We present in this paper the results of an Hα imaging survey of 32 ringed galaxies covering a range of properties and morphologies. The data sample is described in § 2.1, and the observations are described in § 2.2. A verbal description of the characteristics of the distribution of H II regions in each sample galaxy is given in § 3. In § 4, the H II

[1] University of Alabama, Tuscaloosa, AL 35487.
[2] Rhodes College, Memphis, TN 38112.

regions are analyzed for luminosities, luminosity functions, and their distribution around rings. A discussion is presented in § 5, and the conclusions are presented in § 6.

2. DATA

2.1. *The Sample of Ringed Galaxies*

The galaxies in our sample are summarized in Table 1. The galaxies were chosen for a variety of reasons, the main one being that each is an exceptional example of one or more of the different types of ring and pseudoring phenomena described in the CSRG. The sample is therefore not statistical in nature. Both barred and nonbarred galaxies are included, and all are taken from the CSRG with the exception of NGC 210, NGC 1832, and UGC 12646. The types range from $S0^+$ to Sc and are either from CSRG or on the CSRG system, which is a modified version of the de Vaucouleurs (1959) classification system. Corrected magnitudes and heliocentric radial velocities are from the Third Reference Catalog of Bright Galaxies (RC3; de Vaucouleurs et al. 1991). Distances are based on the radial velocity and the linear Virgocentric flow model of Aaronson et al. (1982) or are taken directly from Tully (1988) when possible. These distances are mostly consistent with a Hubble constant of 75 km s^{-1} Mpc^{-1}.

One galaxy included in the sample, ESO 235−58, may be related to polar rings (Buta & Crocker 1993b). We present here Hα+[N II] and red continuum images but no analysis of the H II regions detected.

2.2. *Observations and Calibrations*

The observations were taken in 1993 August using a Tektronix 1024 × 1024 CCD attached to the Cerro Tololo Inter-American Observatory (CTIO) 1.5 m telescope. Seeing during the run was typically around 1".5. The interference filters used were 80 Å wide and centered approximately at 6477, 6563, 6606, 6649, 6693, and 6737 Å. The continuum images were all taken at 6477 Å. Images were flat-fielded with combined dome and twilight flats. The processing of the images prior to calibration and H II region measurement was handled in a nearly standard fashion using tasks in IRAF.[3] The only nonstandard part of the observations was a problem with the CCD readout electronics which had a tendency to introduce a horizontal stripe pattern. This was deemed to be a problem with the older controller which we were using (pre-ARCON) and was treated as a bias problem. We were able to destripe the images using the IRAF task BACKGROUND. This served

[3] IRAF is distributed by National Optical Astronomy Observatories, which is operated by the Association of Universities for Research in Astronomy, under a contract with the National Science Foundation.

TABLE 1

GALAXY SAMPLE[a]

Name	Type	Type Source	B_T^0	$v_\odot$ (km s^{-1})	Δ^b (Mpc)	$M_T^0(B)$
NGC 53	(R′)SB(r)ab	CSRG	13:.20	4568	57.3	−20.6
NGC 210	(R'_2)SAB(s)b	RC3[c]	11.32	1635	20.3	−20.2
NGC 1291	($R_1R'_2$)SB(l)0/a	CSRG	9.32	837	8.6	−20.4
NGC 1317	(R′)SA<u>B</u>(rl)0/a	CSRG	11.81	1941	16.9	−19.3
NGC 1326	(R_1)SB(rl)0/a	CSRG	11.25	1362	16.9	−19.9
NGC 1350	(R'_1)SB(r)ab	CSRG	10.87	1883	16.9	−20.3
NGC 1433	(R'_1)SB(<u>rs</u>)ab	CSRG	10.64	1068	11.6	−19.7
NGC 1832	SB(r)bc	RC3	11.59	1939	23.5	−20.3
NGC 6300	SB(<u>rs</u>)b	CSRG	10.20	1109	14.3	−20.6
NGC 6753	(R′)SA(r)b	CSRG	11.58	3142	39.2	−21.4
NGC 6761	(R′)SB(r)0/a	CSRG	13.63	5650	73.0	−20.7
NGC 6782	(R'_1)SB(r)0/a	CSRG	12.21	3892	49.0	−21.2
NGC 6902	SA(r)b	CSRG	11.58	2785	35.7	−21.2
NGC 6932	(R_1)S<u>A</u>B(r)0^+	CSRG	12.99	3774	46.7	−20.4
NGC 6935	(R)SA(r)a	CSRG	12.65	4691	60.0	−21.2
NGC 6937	(R′:)SB(r)c	CSRG	13.35	4663	59.6	−20.5
NGC 7020	(R)SA(r)0^+	CSRG	12.67	2978	37.8	−20.2
NGC 7098	(R)SA<u>B</u>(r)a	CSRG	11.63	2399	29.1	−20.7
NGC 7187	(R)S<u>A</u>B(r)0^+	CSRG	13.42	2670	33.9	−19.2
NGC 7219	(R'_2)SA(r)b	CSRG	13.07	2930	35.7	−19.7
NGC 7267	(R'_1)SB(rs)a	CSRG	12.80	3346	42.8	−20.4
NGC 7329	SB(r)b	CSRG	12.03	3159	38.6	−20.9
NGC 7417	(R′)SB(r)a	CSRG	12.93	3196	39.1	−20.0
NGC 7531	S<u>A</u>B(r)bc	CSRG	11.41	1595	19.3	−20.0
NGC 7702	(R)SA(r)0^+	CSRG	13.03	3122	38.3	−19.9
IC 1438	($R_1R'_2$)SA<u>B</u>(r)a	CSRG	12.46	2616	33.8	−20.2
IC 4754	(R′)SB(r)ab	CSRG	13.79	4950	63.0	−20.2
IC 5240	SB(r)ab	CSRG	12.29	1773	21.4	−19.4
UGC 12646	(R'_1)SB(r)ab	RC3[c]	13.67	8033	108.9	−21.5
ESO 111−10.....	(R'_1)SAB(rs)b	CSRG	13.77	4829	60.9	−20.2
ESO 152−26.....	($R_1R'_2$)S<u>A</u>B(r)ab	CSRG	13.85	6065	77.2	−20.6
ESO 235−58.....	(PR?)SB:(rs:)cd: p	CSRG	14.82	4308	55.0	−18.9

[a] Magnitudes and radial velocities from RC3.

[b] Distances either from Tully 1988 or computed from linear Virgocentric flow model (Aaronson et al. 1982).

[c] RC3, Appendix 3.

also to subtract the sky background, after which the continuum could be scaled to the Hα image using field stars, then subtracted. Field stars were used to align the images as well.

The calibration to apparent flux follows the technique outlined in Jacoby, Quigley, & Africano (1987). Standard stars were observed in all the passbands, several times each night. The total flux for each standard star was measured in a simulated 20″ diameter aperture. Transmission curves for the filters were acquired from the CTIO archives. Correction for atmospheric extinction was made using the standard CTIO extinction curve. The formal errors in the sensitivity solutions over all the nights were of order 1%–3%, reinforcing our impressions that the nights of the observations were nearly photometric. The final filter sensitivities used were the values averaged over all the nights.

The accuracy of our calibrations was checked by observing planetary nebulae having accurately known Hα and [N II] fluxes from Kohoutek & Martin (1981). For this purpose, we used IC 418, NGC 6326, and NGC 6818. IC 418 was observed on four nights, NGC 6818 on two nights, and NGC 6326 on one night. The images of these objects were reduced in the same manner as the galaxy images and calibrated using the same standard stars. The fluxes derived for IC 418 snd NGC 6818 on the different nights showed excellent internal consistency, differing only by at most 0.01 dex from night to night. However, the analysis showed that our calibration gave fluxes too bright by 0.13 ± 0.02 dex. The consistency between the three planetary nebulae and the internal consistency on different nights suggests that we can apply this to the galaxy logarithmic fluxes mainly as a zero-point correction. Thus, all logarithmic Hα+[N II] fluxes in this paper have been reduced by 0.13.

3. DESCRIPTIONS OF Hα DISTRIBUTIONS IN RINGED GALAXIES

Our sample of 32 ringed galaxies shows much diversity in Hα properties. The galaxies are all illustrated in Figures 1–11 (Plates 24–34), where each image is oriented with north at the top and east to the left. The scale bar at lower left on each continuum image is 30″ in length. In Figure 12 (Plate 35), the nuclear regions in 12 galaxies are shown on a larger scale (scale bar in lower left of each panel is 5″ in length). Let us describe first the properties of the H II region distribution in each case, after which the properties of the H II regions will be analyzed.

NGC 53 (Fig. 1, *top*).—The H II regions are concentrated mainly in the bright inner ring. The interior of the ring is mostly devoid of emission, except for the central area. The asymmetry just off the north side of the ring includes bright H II regions. Only a few very faint H II regions are in the outer pseudoring region.

NGC 210 (Fig. 1, *middle*).—H II regions line the prominent R'_2 outer pseudoring. There are also a few interarm H II regions. The oval bar region has a clear spiral pattern of H II regions (see expanded image in Fig. 12). The dust lanes in the oval (see Sandage 1961 and Sandage & Bedke 1994) are on the inner sides of the Hα arms. The bright central emission is not ringlike.

NGC 1291 (Fig. 1, *bottom*).—The Hα distribution is diffuse and spiral-like in the bar/lens region; this region is not covered by the field studied by Caldwell et al. (1991). The morphology in the bar/lens region is not obviously correlated with the optical structure. Weak Hα arms extend beyond the inner lens. Discrete H II regions are found mainly in the outer ring, which extends beyond the boundaries of the field. The emission near the center is asymmetric (see Fig. 12), and there is some slight core saturation. None of the other galaxies in our sample show the complex structure of ionized gas as in NGC 1291, but also most of the other galaxies do not appear to be as bulge-dominated as NGC 1291. More information on the diffuse emission in NGC 1291 is provided in § 5.

NGC 1317 (Fig. 2, *top*).—This is a face-on peculiar spiral near Fornax A (NGC 1316). Hα emission is concentrated in a *double nuclear ring/pseudoring morphology* which is best illustrated in the close-up in Figure 12. The inner nuclear ring is oval and is aligned nearly perpendicular to the fat primary bar (see § 4.5). There is a bright nuclear bar inside this ring; it is not visible in the continuum image in Figure 2, but it is well illustrated by Schweizer (1980). The outer nuclear pseudoring is nearly circular. There is bright central emission, and there is faint diffuse emission inside the inner nuclear ring. Only a few much fainter H II regions are detected outside the nuclear rings. These are near the boundary of the inner lens recognized in the CSRG.

NGC 1326 (Fig. 2, *middle*).—The inner and outer rings in this object are exceptionally clear examples. The object has only a weak bar, however. The outer Hα structure does *not* follow the outer ring. The H II regions near and beyond the outer ring, which is type R_1 in the notation of Buta & Crocker (1991), begin nearly along the bar line and lead it slightly. The Hα spiral arms also end slightly ahead of the bar; they stay mostly outside the R_1 and go well beyond this feature. The appearance of the outer Hα arms is consistent with the R'_2 morphology illustrated in Buta & Crocker (1991), but only 180° of each arm is populated with clear H II regions. The continuum image is dominated by the R_1 component of an $R_1R'_2$ morphology. A bright H II region is located at the southern dimple of the R_1 component. The galaxy is located in the Fornax Cluster, so the slight asymmetry of the outer arms may be due to some weak interaction.

In the inner regions, the emission is very bright and mostly ringlike (see Fig. 12). Discrete H II regions line this nuclear ring, which is also detectable in blue light (Buta & Crocker 1991). The ring is asymmetrically bright and may be affected by extinction. A detailed multiwavelength study of this ring is given by Garcia-Barreto et al. (1991). In the bar region, there is one bright H II region at the south end. A few other very faint H II regions are scattered in the inner lens region, and the inner ring is *not* prominent at all in Hα.

NGC 1350 (Fig. 2, *bottom*).—The inner ring, though prominent in the red continuum image, is only sparsely lined with H II regions. There are two opposing bunches of H II regions near and slightly leading the bar ends. A few H II regions are scattered within the inner ring. The H II regions in the outer arms are concentrated in arcs around the bar axis. Apparent patches of diffuse emission are due to scattered light from a bright foreground star. Some of the outer H II regions may be associated with secondary arcs like those which lead the bar in NGC 1433. There are very few H II regions in the major axis quadrants of the outer pseudoring, which is type R'_1.

NGC 1433 (Fig. 3, *top*).—Discrete H II regions line about three-quarters of the inner ring and are most concentrated near the bar ends. They scatter in and around the spiral arcs which overshoot the bar. The two outer secondary arcs

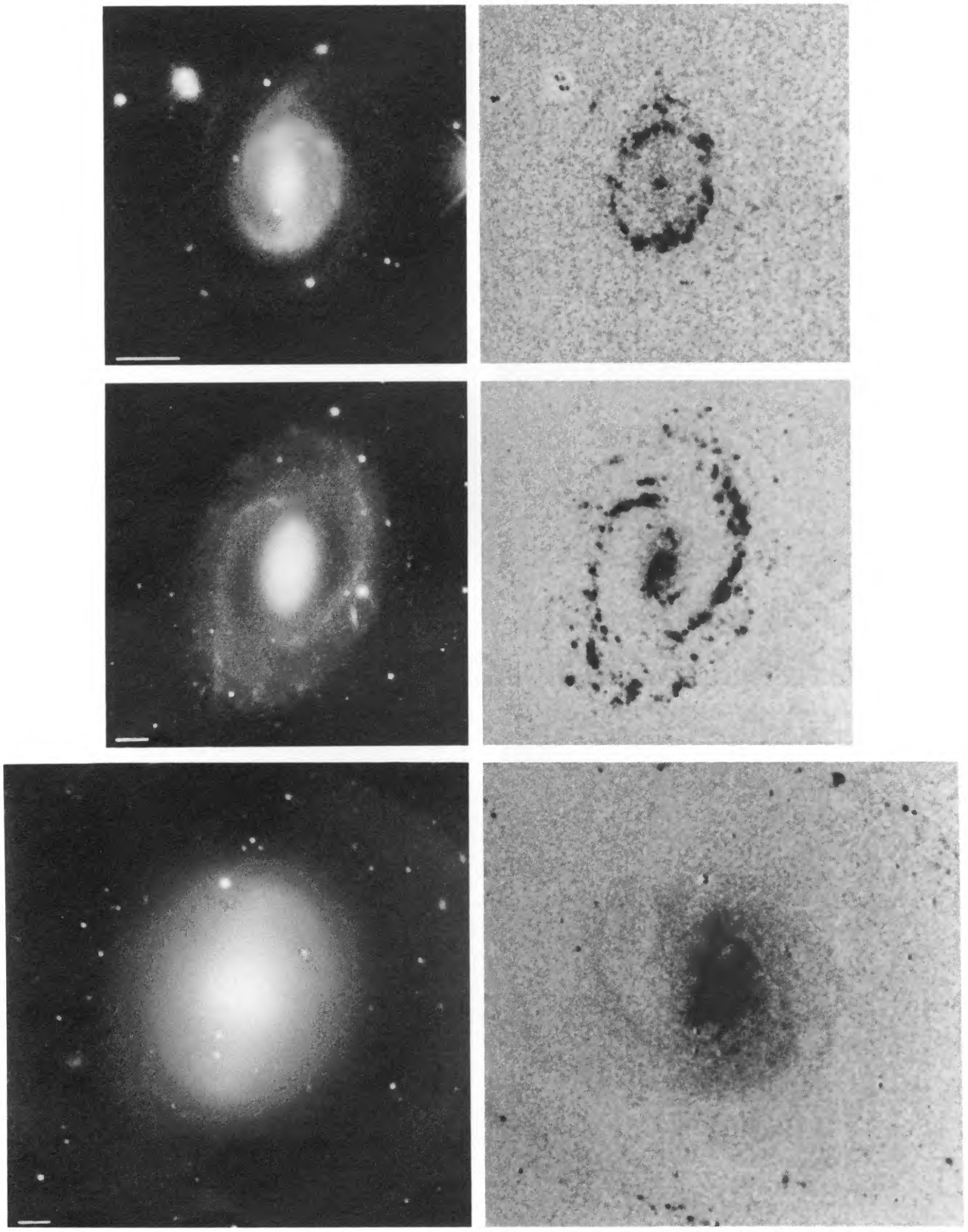

FIG. 1.—Red continuum (6477 Å, *left*) and Hα + [N II] images (*right*) of NGC 53 (*top panels*), NGC 210 (*middle panels*), and NGC 1291 (*bottom panels*). The white bar at lower left in each continuum image is 30″ in length. North is at the top and east is at the left in each image.

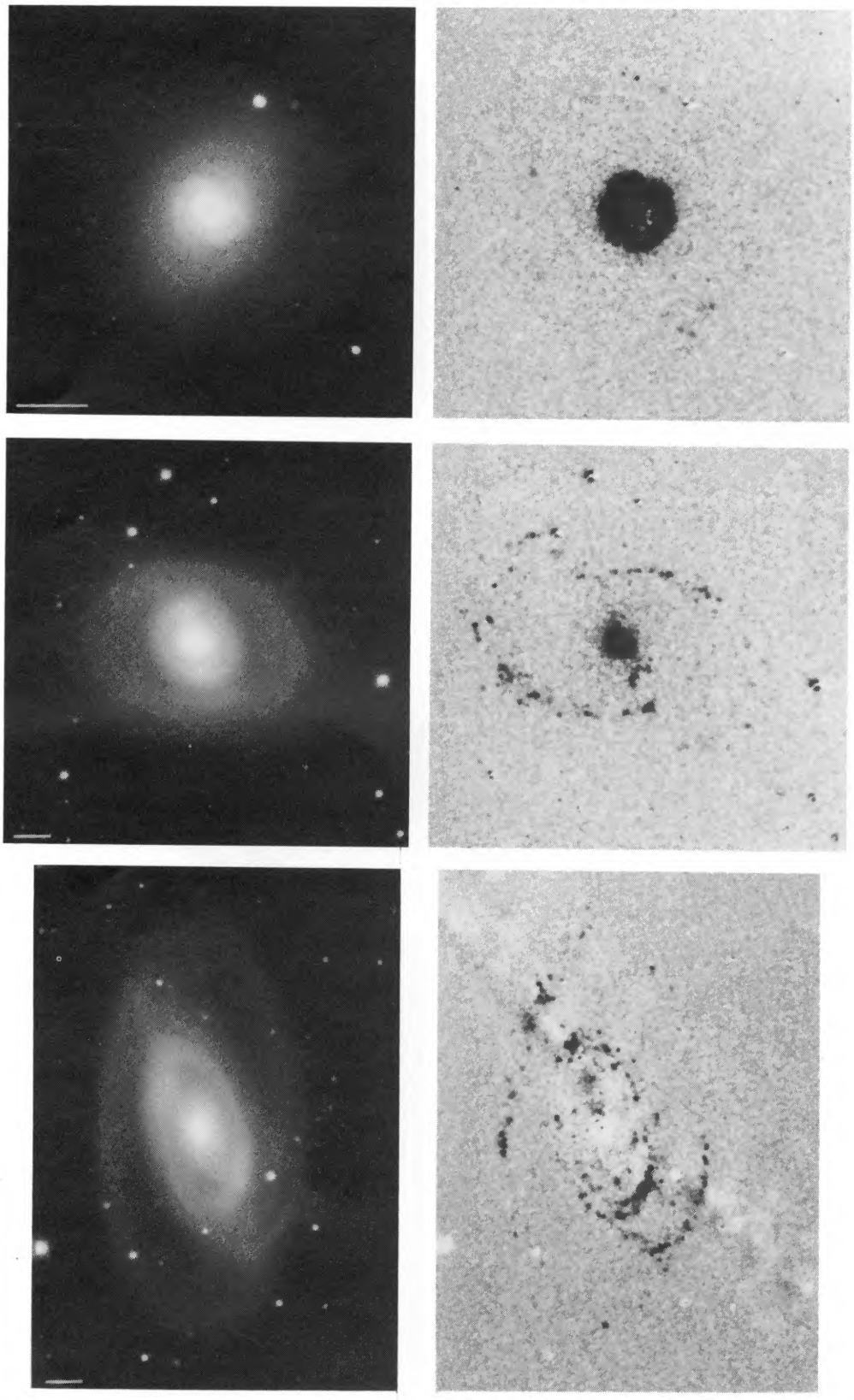

FIG. 2.—Same as Figure 1 for NGC 1317 (*top panels*), NGC 1326 (*middle panels*), and NGC 1350 (*bottom panels*). In the NGC 1350 images, scattered light from a bright foreground star has caused the bright and dark streaks.

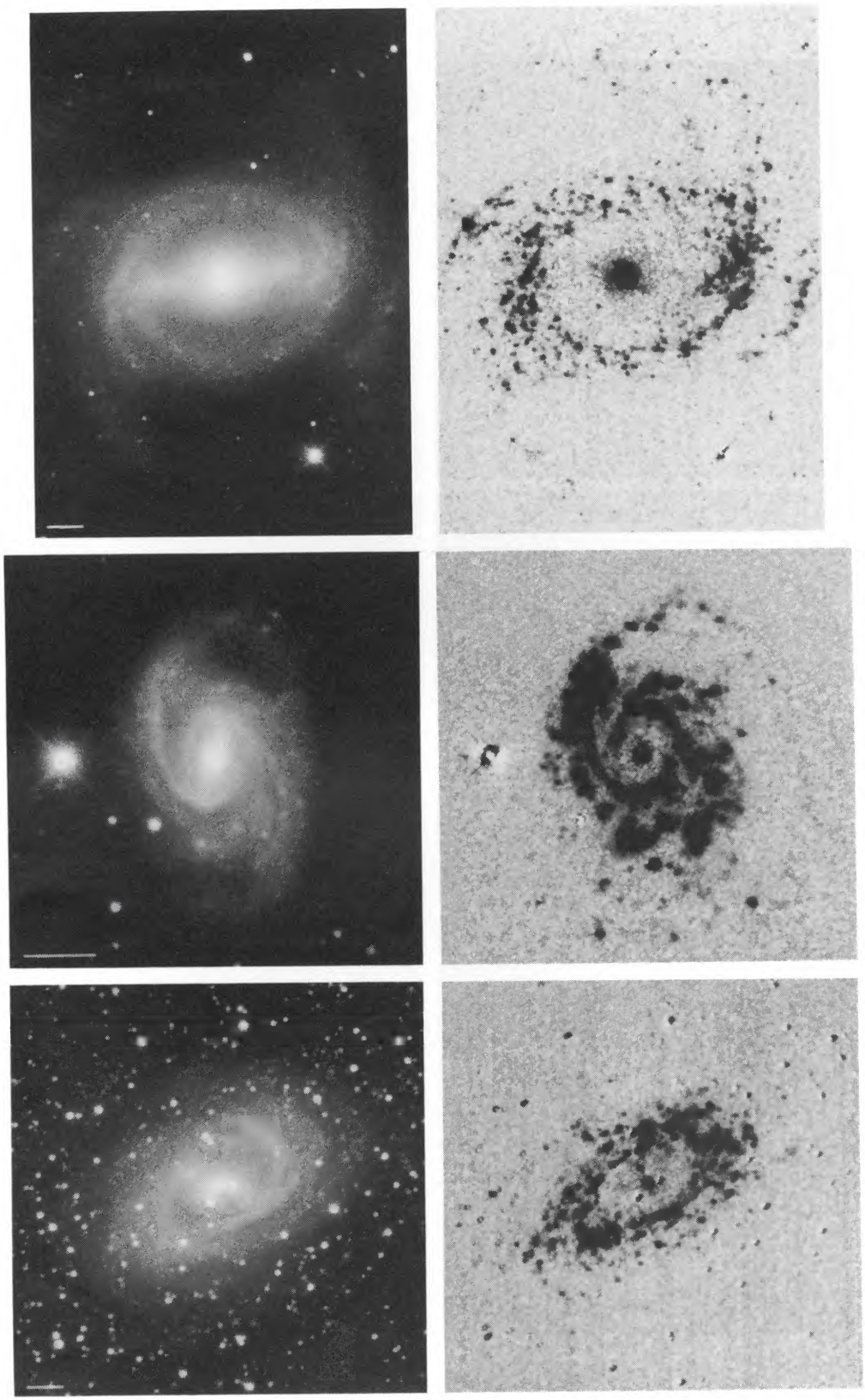

FIG. 3.—Same as Fig. 1 for NGC 1433 (*top panels*), NGC 1832 (*middle panels*), and NGC 6300 (*bottom panels*)

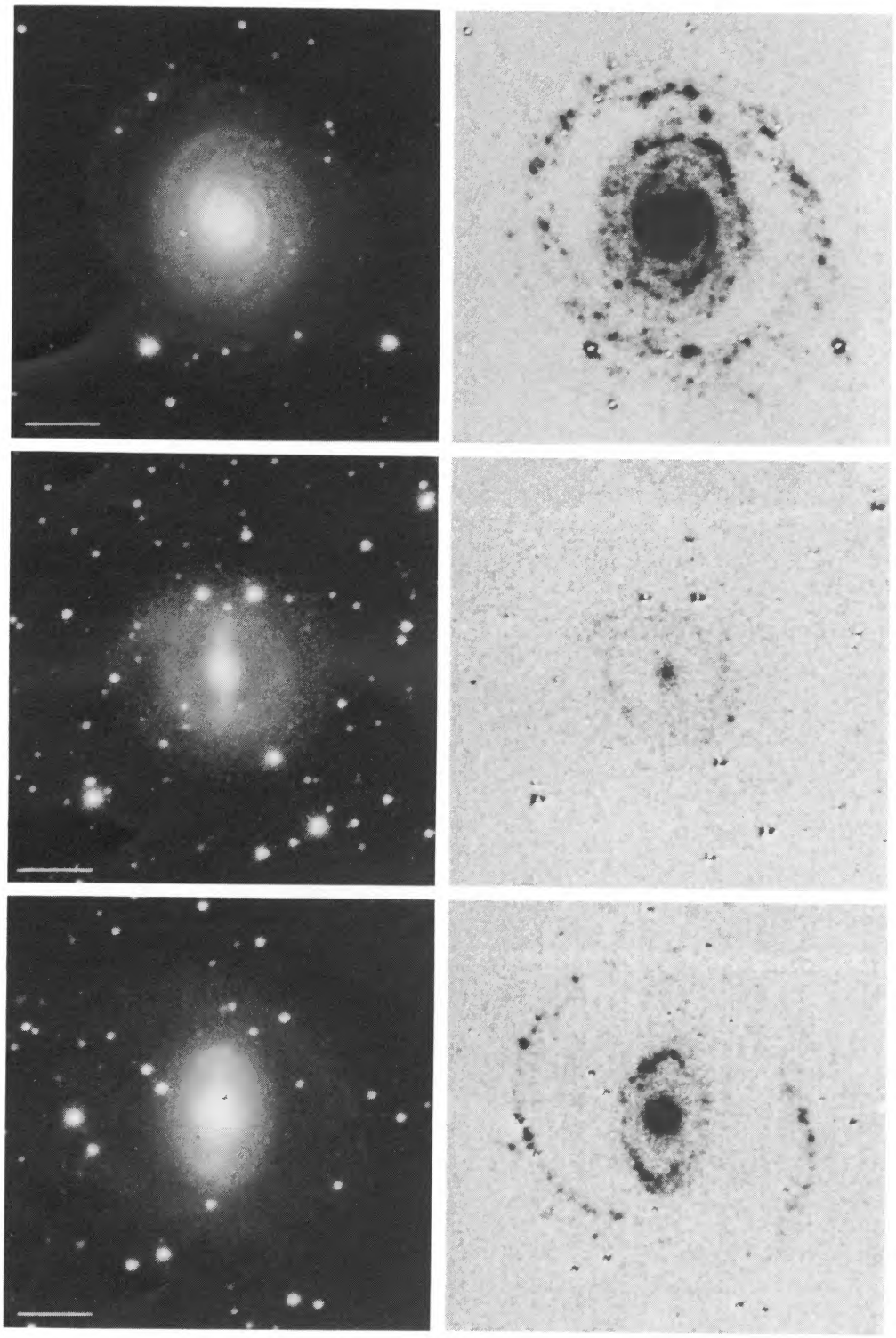

FIG. 4.—Same as Fig. 1 for NGC 6753 (*top panels*), NGC 6761 (*middle panels*), and NGC 6782 (*bottom panels*)

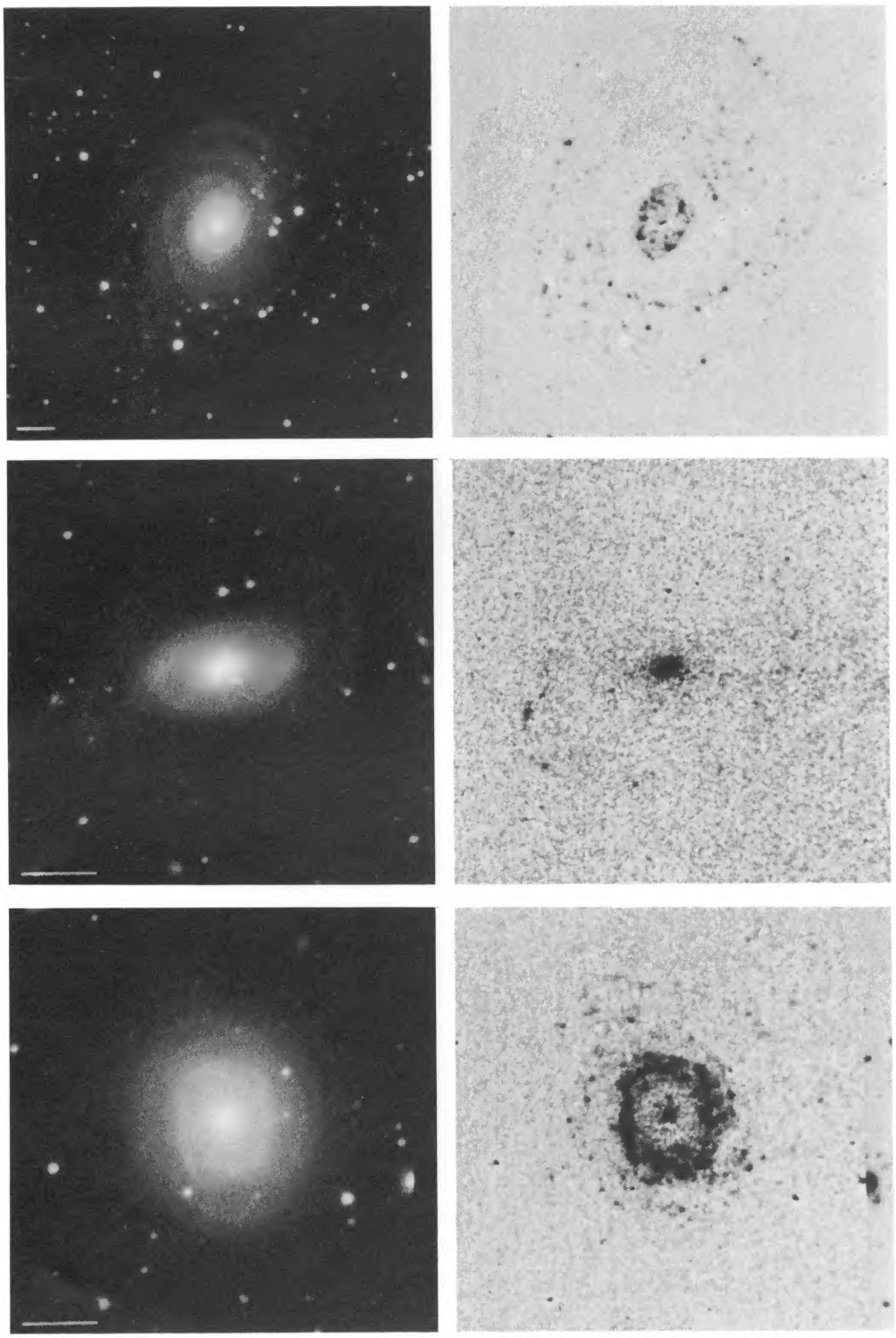

FIG. 5.—Same as Fig. 1 for NGC 6902 (*top panels*), NGC 6932 (*middle panels*), and NGC 6935 (*bottom panels*)

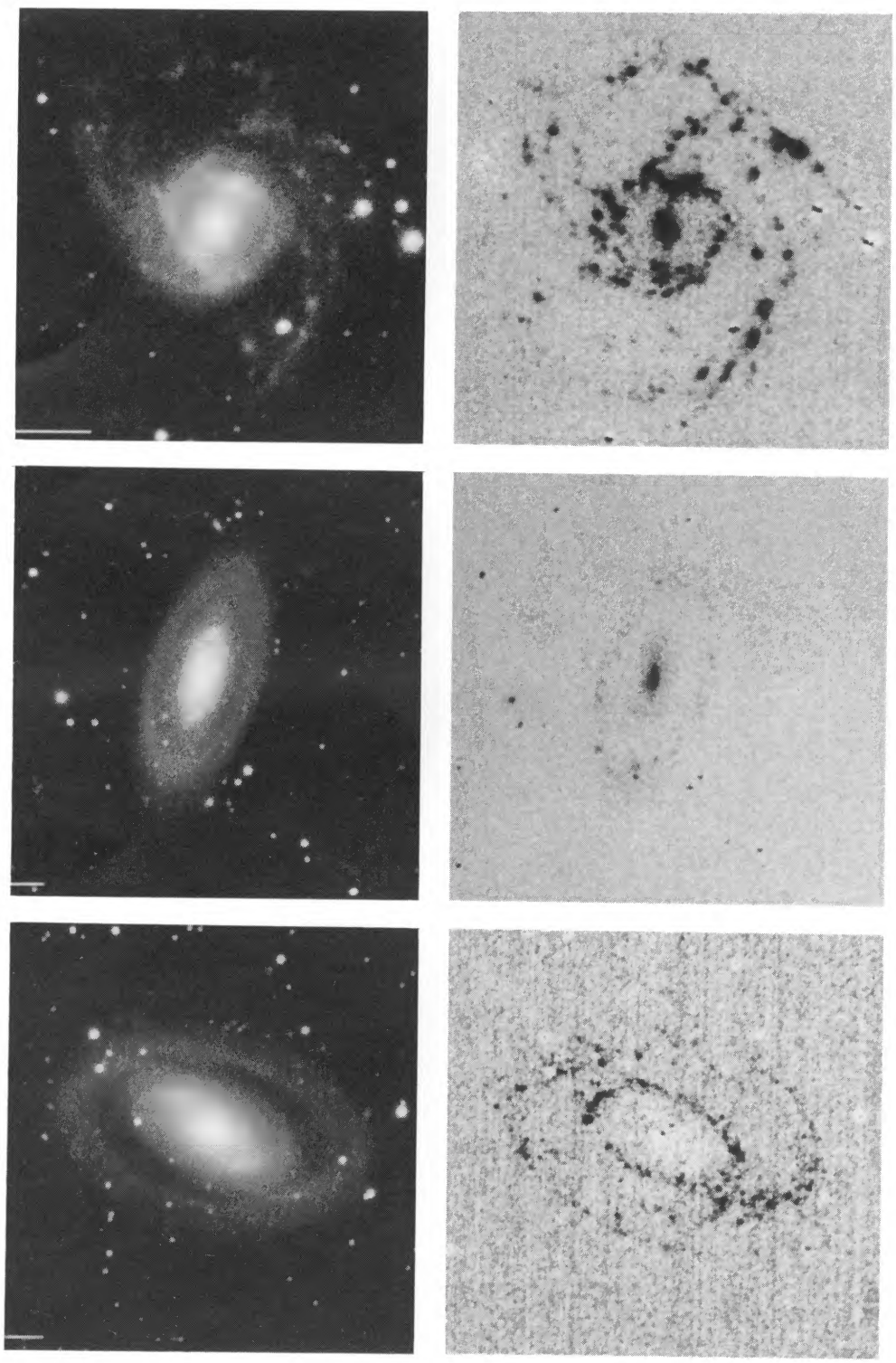

FIG. 6.—Same as Fig. 1 for NGC 6937 (*top panels*), NGC 7020 (*middle panels*), and NGC 7098 (*bottom panels*)

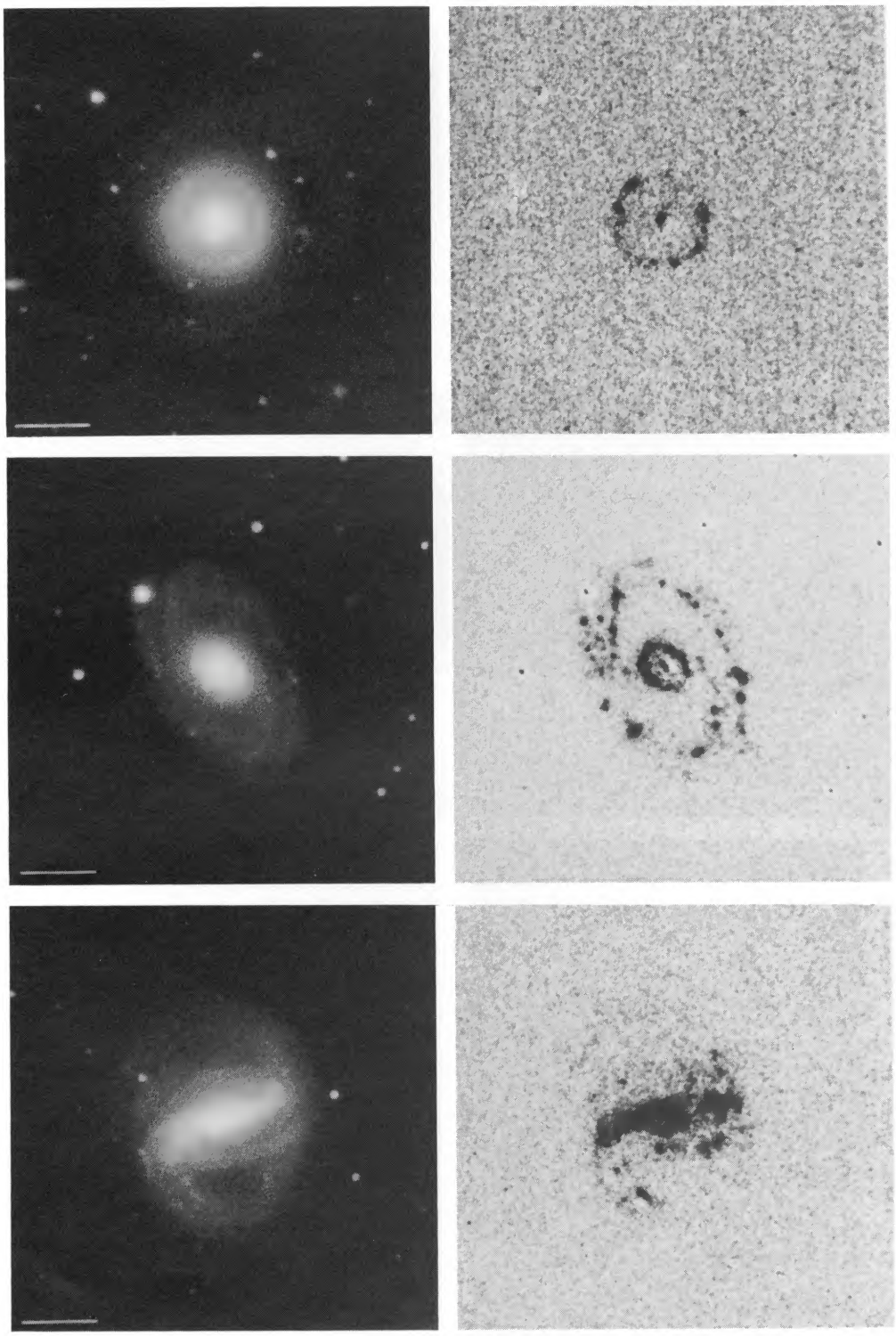

FIG. 7.—Same as Fig. 1 for NGC 7187 (*top panels*), NGC 7219 (*middle panels*), and NGC 7267 (*bottom panels*)

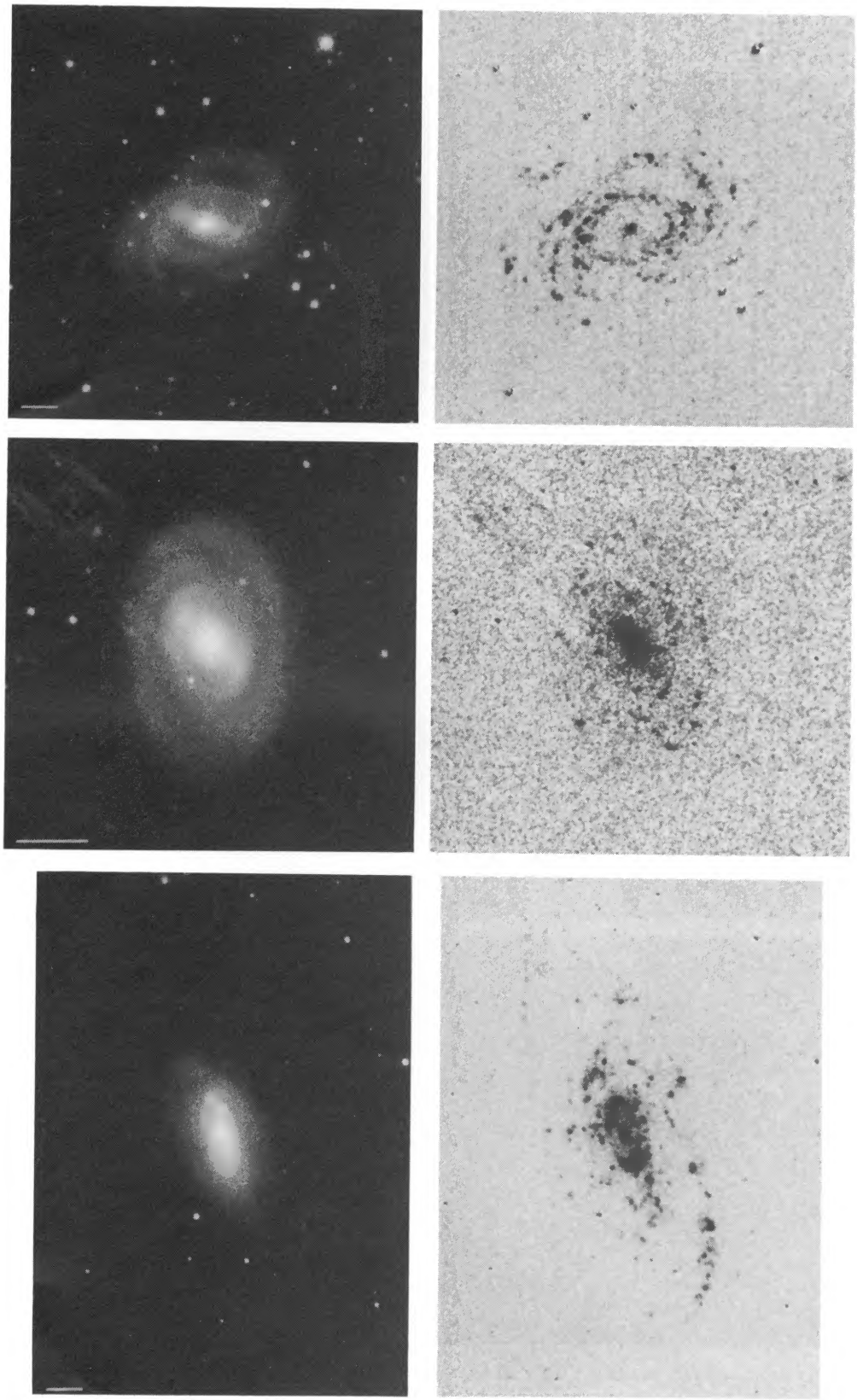

FIG. 8.—Same as Fig. 1 for NGC 7329 (*top panels*), NGC 7417 (*middle panels*), and NGC 7531 (*bottom panels*)

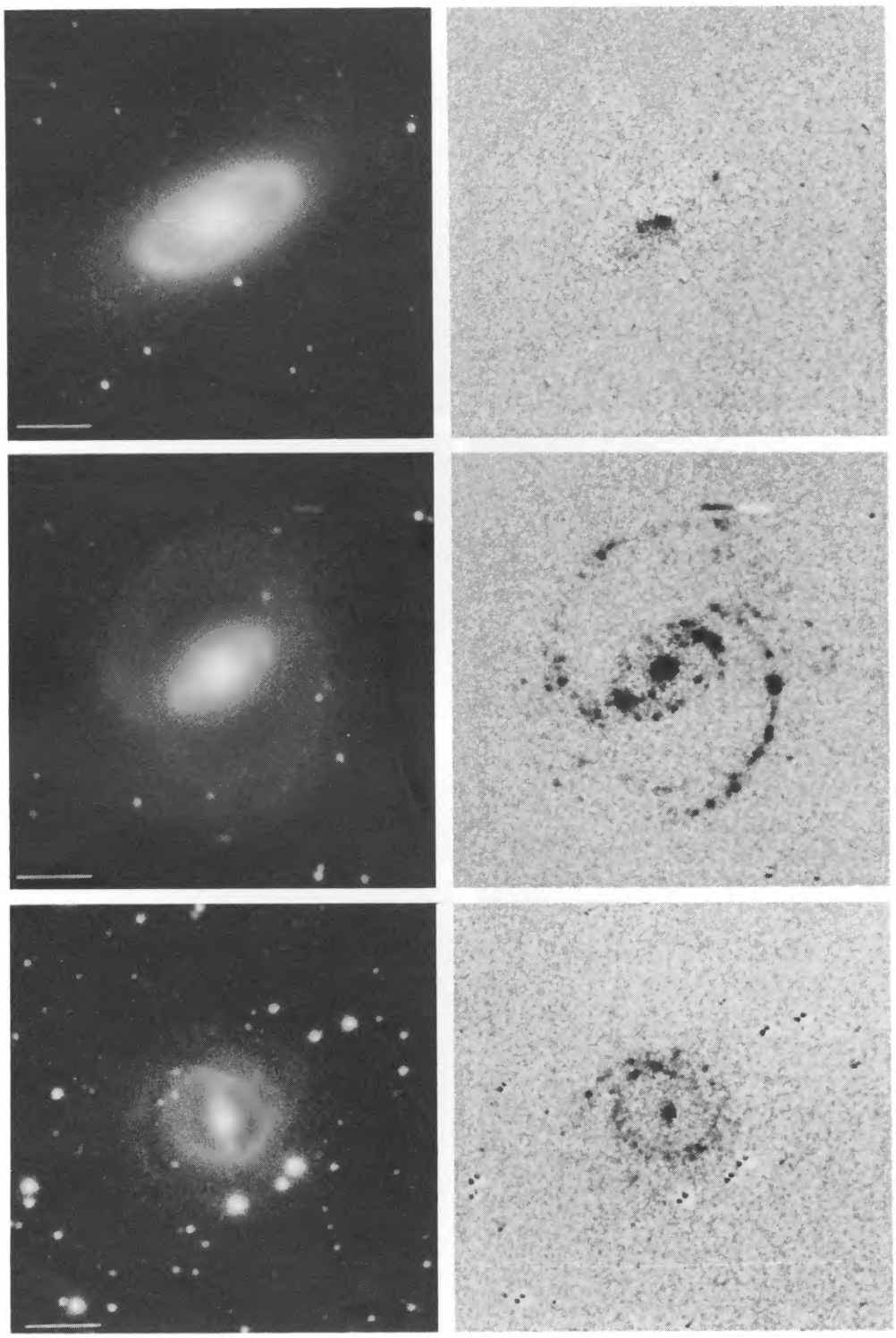

FIG. 9.—Same as Fig. 1 for NGC 7702 (*top panels*), IC 1438 (*middle panels*), and IC 4754 (*bottom panels*)

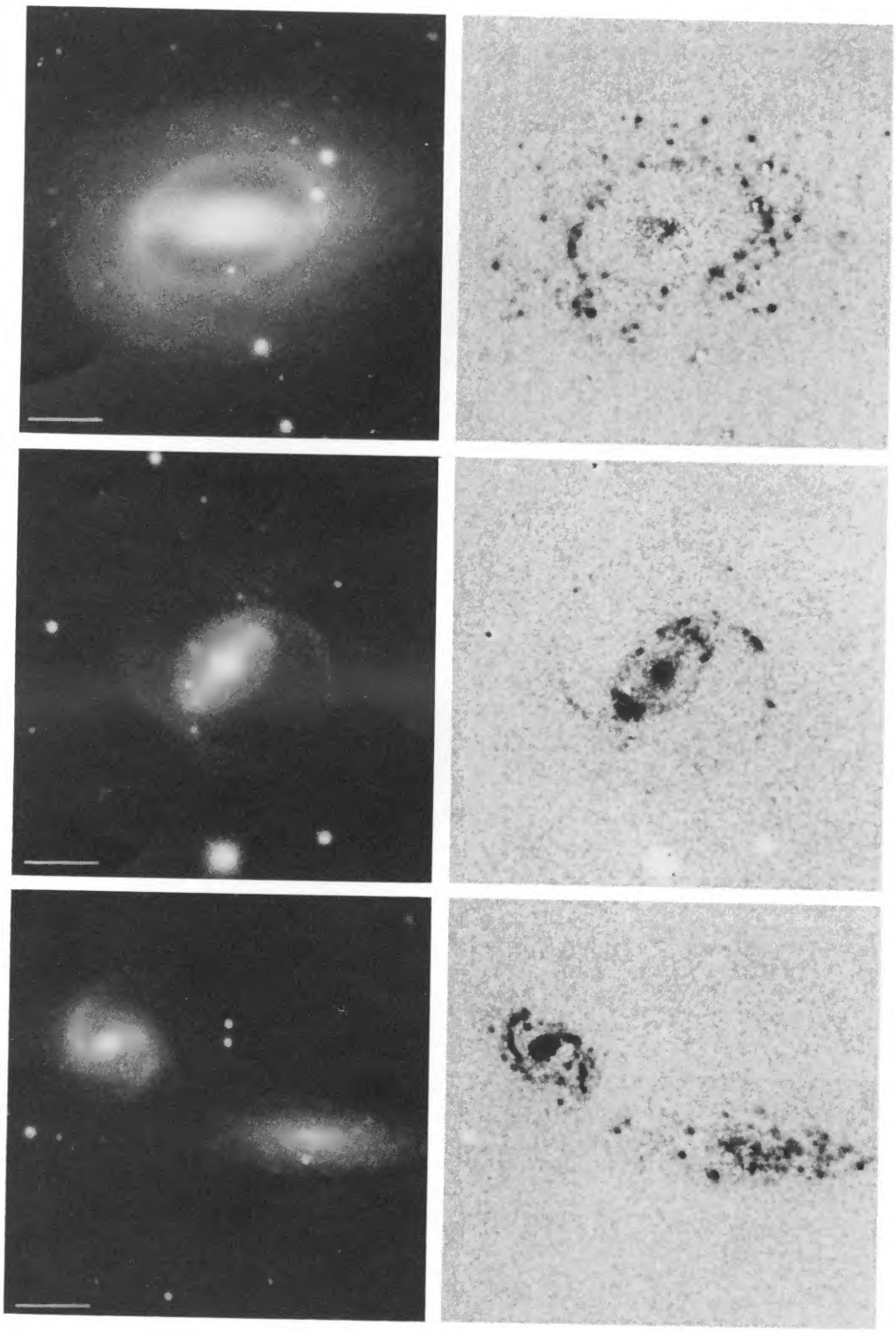

FIG. 10.—Same as Fig. 1 for IC 5240 (*top panels*), UGC 12646 (*middle panels*), and ESO 111−10 (*bottom panels; left of two*) and ESO 111−9 (*bottom panels; right of two*)

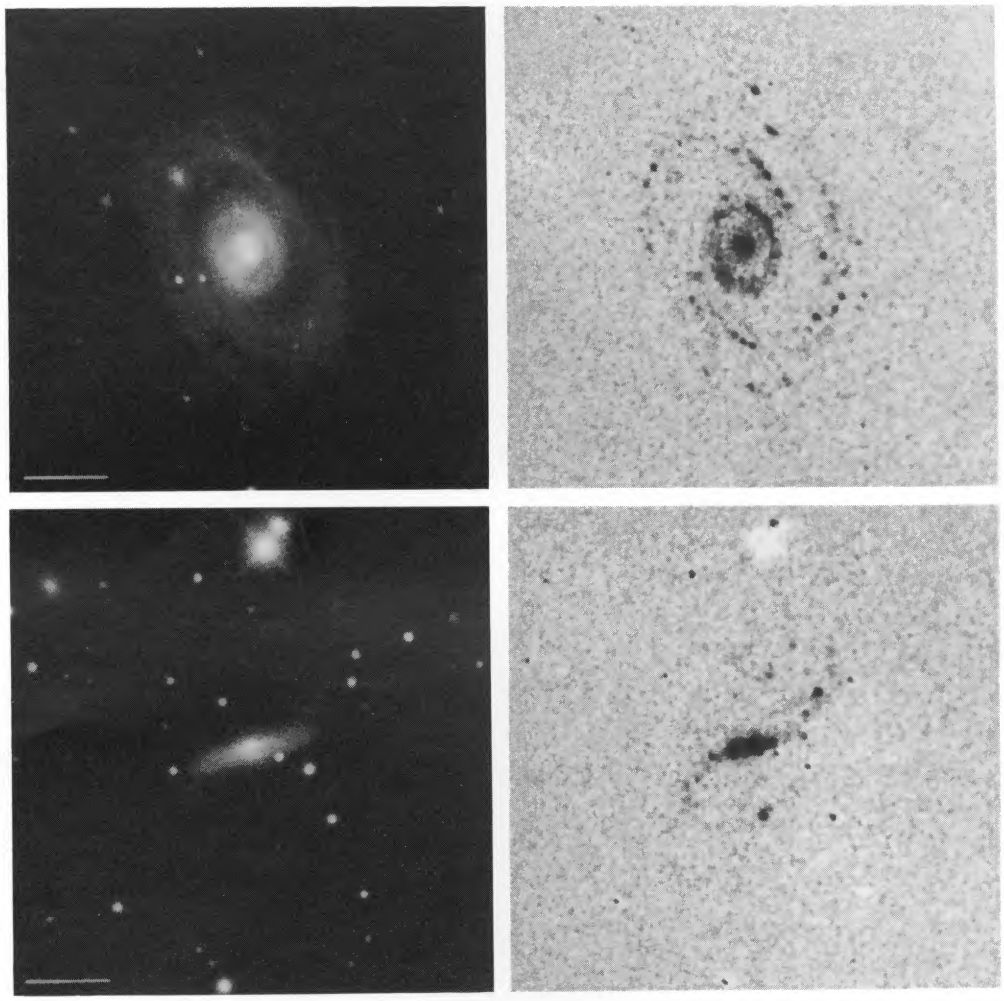

FIG. 11.—Same as Fig. 1 for ESO 152−26 (*top panels*) and ESO 235−58 (*bottom panels*)

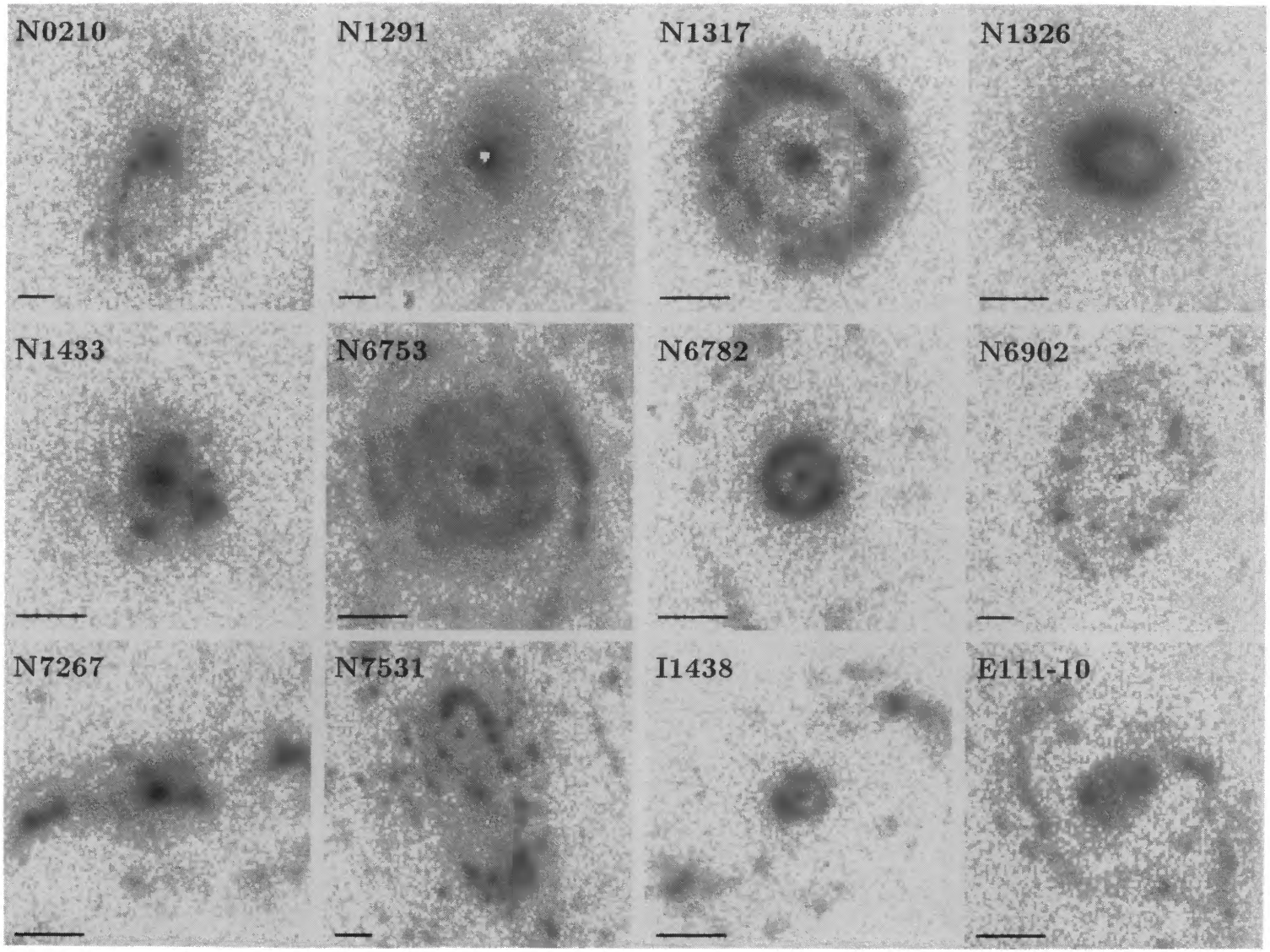

FIG. 12.—Montage of Hα + [N II] images of the central regions of 12 ringed and pseudoringed galaxies. The dark scale bar at lower left in each image is 5″ in length. North is at the top and east is to the left in each image. The central few pixels in the NGC 1291 image suffered saturation in the CCD readout.

CROCKER, BAUGUS, & BUTA (see 105, 355)

(called "plumes" by Buta 1986) are lined by H II regions. One of the brightest H II regions lies at the center of the eastern "plume" and is ring-shaped; this object is 4".9 in angular diameter and is located 42".8 north and 131".3 east of the nucleus. The eastern plume also has two additional arcs of H II regions. The western plume has a "hanging" H II region between it and the inner ring. In the outer pseudoring, H II regions are very few and very faint. There are a few H II regions inside the inner ring, scattered in the lens region (not in the bar itself). The nuclear region (shown at large scale in Fig. 12) has a few bright discrete H II regions, a bright center of emission, and diffuse emission. The fainter H II regions distribute here in a nearly circular ring around the nucleus. The structure is similar to that in NGC 1317. The diffuse emission in this region resembles the nuclear continuum oval.

NGC 1832 (Fig. 3, *middle*).—Many bright H II regions lie outside the inner ring, distributed in bright spiral arms. The inner ring is a pseudoring in Hα. There is bright central emission but no H II regions between the center and the inner ring. The inner arms are part of a spiral oval, of the NGC 5248 type. The continuum image does not show the bright single outer arm on the west side, which indicates a probable interaction.

NGC 6300 (Fig. 3, *bottom*).—H II regions concentrate along and just outside the inner pseudoring (see also Ryder & Dopita 1993). They extend into the diffuse outer disk region and do *not* concentrate at the bar ends. Instead, they concentrate nearly perpendicular to the bar. There is one bright H II region in the northeast side of the bar located near a dust lane. The region inside of the ring is mostly devoid of H II regions, except for intense nuclear emission.

NGC 6753 (Fig. 4, *top*).—In the continuum image we see (1) a nuclear ring-lens, (2) a pseudoring just outside this lens, (3) an intermediate zone of spiral structure, like a pseudo-ring at the rim; and (4) an outer pseudoring. H II regions and diffuse emission concentrate in the nuclear ring-lens (see large-scale view in Fig. 12). Feature (2) is not a ring or pseudoring in Hα. In zone (3) we see Hα arms and a pseudoring character. The outer pseudoring is well defined in Hα, and there is not much emission beyond it. There is bright central emission.

NGC 6761 (Fig. 4, *middle*).—Hα emission is very faint, but the inner ring is clear as a virtually continuous feature. The ring is uniform, and the bar ends are not distinguishable. There are two symmetric short arms of Hα emission outside of the inner ring; the one on the south side includes an unusually bright H II region compared to those in the inner ring. There is also bright central emission.

NGC 6782 (Fig. 4, *bottom*).—Excellent three-ring system (see Byrd et al. 1994; CSRG). The outer arms form an R'_1 outer pseudoring in blue light. H II regions line the south to east portion of the R'_1, and there is an arc of H II regions on the western half of the R'_1. The feature is not symmetric in Hα, but it appears, as in NGC 1326, that the very faint H II regions in the northeast and southwest outer quadrants are following an R'_2 morphology.

The inner ring is very pointy in the red continuum image, and this characteristic is also evident in Hα. The H II regions in the inner ring are bright around the cusps, which coincide with the bar ends. At the ring minor axis, the emission is very faint, although there are a few H II regions. H II regions in the inner ring are mostly bunched up around the ring major axis.

The nuclear ring includes the brightest Hα emission (see the close-up view in Fig. 12). Discrete H II regions and diffuse emission line a nearly circular feature. There is nuclear emission that is fainter than the nuclear ring H II regions. The ring is *not* doubled as in NGC 1317. In a $B-I$ color index map, the nuclear ring stands out as a very blue feature (see Fig. 24 of the CSRG).

NGC 6902 (Fig. 5, *top*).—In blue light, this is a conspicuous multiarmed ringed spiral. In the continuum image, the inner ring is very bright. In Hα, the ring has H II regions well distributed in azimuth (see close-up view of this region in Fig. 12). There are bright H II regions at the ends of a very weak bar inside the inner ring. There are also bright H II regions nearly perpendicular to this bar. The outer arms have many scattered H II regions. There is a very faint nuclear emission source, and there is diffuse emission inside the inner ring.

NGC 6932 (Fig. 5, *middle*).—The few discrete H II regions in this galaxy are in the outer ring, which is very faint in the continuum image (an image which shows this feature better is displayed in Fig. 31 of the CSRG). The H II regions are not associated with the weak dimpling in this ring. There is bright central emission but little Hα emission from the inner ring.

NGC 6935 (Fig. 5, *bottom*).—The inner ring is well defined in Hα and is very boxy. Numerous faint H II regions are outside this ring. There is diffuse emission inside the ring, and there is bright central emission. Except for the boxiness of the inner ring, the distribution of H II regions resembles what is seen in NGC 7742 (Pogge & Eskridge 1993).

NGC 6937 (Fig. 6, *top*).—The central part of the bar is bright in Hα. The inner ring is lined with H II regions. The north end of the bar has bright H II regions, but the south end has nothing. The outer arms are asymmetric. This galaxy is close to NGC 6935 and may be suffering an interaction.

NGC 7020 (Fig. 6, *middle*).—Hα emission is confined to the bright outer ring and the center. There could be emission from one of the "ansae" in the inner hexagonal zone. The central emission is very extended and may fill most of the inner hexagonal zone. This object is illustrated and discussed in Buta (1990b), the CSRG, and Wozniak et al. (1995).

NGC 7098 (Fig. 6, *bottom*).—H II regions line the inner ring and various parts of the outer ring and arms. The bright bar ansae have *no* associated emission. The two brightest H II regions in the inner ring are significantly offset from the bar ends; they trail the bar at an intermediate point. Near the south dimple in the outer ring, there are two bright H II regions. The central emission may be spurious. The galaxy is also illustrated and discussed in the CSRG.

NGC 7187 (Fig. 7, *top*).—A very weak bar crosses the bright inner ring in the red continuum image. H II regions line about two-thirds of the ring. These are brightest near the bar ends. There is only one clear H II region in the very faint outer ring, and there is significant nuclear emission. The galaxy is also discussed by Buta (1990a) and Wozniak et al. (1995).

NGC 7219 (Fig. 7, *middle*).—The inner ring is very bright in Hα. It is brightest in arcs around a very weak bar, barely visible in the continuum image. The R'_2 outer pseudoring recognized in the CSRG is lined by bright H II regions. The Hα arms begin along the bar axis, and the brightest H II

region in the galaxy is in one of these outer arms. The nuclear emission may be spurious.

NGC 7267 (Fig. 7, *bottom*).—This is a four-armed barred spiral. The bar is very bright and has complex structure in the continuum, in effect splitting at the ends. The outer pseudoring is of the R'_1 type. In Hα, the dominant feature is the bar. There are bright complexes near the bar ends that do not correlate well with continuum features. No clear ring patterns are evident in Hα. Discrete H II regions and diffuse emission lie around the bar and in one of the outer arms. Details in the bar and central regions are shown better in the close-up in Figure 12. There is an intense nucleus of emission.

NGC 7329 (Fig. 8, *top*).—The bar is bright in this beautiful multiarmed barred spiral. H II regions line the inner ring and complex outer arms. The region interior to the ring is devoid of H II regions. There is bright nuclear emission which may have some structure. The ends of the bar are not special in this case.

NGC 7417 (Fig. 8, *middle*).—The images of this galaxy are affected by scattered light from a bright star just outside the boundaries of the field. There appear to be two barlike gaseous ovals: a nuclear oval (not visible in Fig. 8) 5″ in radius having an axis ratio of 0.51 and oriented at position angle 0°; and a second oval 12″ in radius having an axis ratio of about 0.63 and a position angle of 35° (this one is visible in the right middle panel of Fig. 8). The primary stellar bar visible in the continuum image is oriented at a position angle of 43°; thus, both apparent gaseous ovals are misaligned with the stellar bar. Both ovals lead the primary bar if the outer arms are trailing. The nuclear oval has no stellar counterpart. The galaxy has an inner ring and a bright outer pseudoring. A few discrete H II regions are associated with the inner ring. Many more are in the outer arms. Owing to the effects of the scattered light, no parameters for this galaxy are tabulated here.

NGC 7531 (Fig. 8, *bottom*).—The red continuum image shows only the inner regions but not the outer structure. See Buta (1987a) for deep broadband images of this galaxy. The inner ring is very bright in Hα, as shown in the close-up view in Figure 12. There is obvious diffuse emission inside the ring, and there is bright central emission. Many bright H II regions line the outer arms. The arm nearest the apparent low surface brightness companion (A2311.8−4353) due west is brightest. No H II regions are seen in the region of this object.

NGC 7702 (Fig. 9, *top*).—The bright inner ring is devoid of emission. There is one discrete H II region just inside the inner ring on the northwest side of the major axis. There may be nuclear emission, but its appearance could be affected by a mismatch with the continuum image. There may be diffuse emission associated with a dust patch on one side. The galaxy is discussed further by Buta (1991) and Wozniak et al. (1995).

IC 1438 (Fig. 9, *middle*).—The H II regions in the inner ring are very clumped at the bar ends; away from the bar ends they are much fainter and fewer in number. The outer arms are very bright in Hα in the quadrants trailing the bar only. They follow the R'_2 part of the outer structure most closely, as in NGC 1326 and 6782. The center has a clear nuclear ring of H II regions (see close-up view in Fig. 12). This ring is completely filled with diffuse emission. There is a bright nuclear source also. A few faint H II regions lie on both leading edges of the bar. The outer Hα arms begin nearly along the bar axis. An asteroid passed through the field at the time of the observation and left the streaks to the northwest of the galaxy center.

IC 4754 (Fig. 9, *bottom*).—The bar is strong; this is a possible misaligned bar/ring case noted in the CSRG. The inner ring is lined by H II regions, with the brightest just trailing the bar ends. Two or three short outer arms also have H II regions. There is bright central emission.

IC 5240 (Fig. 10, *top*).—The bright inner ring is lined by discrete H II regions. There are bright ones near each end of the bar. No H II regions are seen inside the ring. There is a bright nuclear source and faint diffuse emission along the bar to the east. Many discrete H II regions scatter in the faint flocculent outer arms.

UGC 12646 (Fig. 10, *middle*).—The inner ring has very bright clumps of H II regions around the bar ends, which coincide with the intrinsic ring major axis. Emission in the ring away from the major axis is much fainter. The bar may have diffuse emission. The trailing quadrants of the R'_1 have some H II regions. The very faint Hα arms do not follow the full R'_1 outer pseudoring (see Fig. 23 of the CSRG) but instead follow a clear R'_2 feature. The central emission is very bright but is not ringlike.

ESO 111−10 (Fig. 10, *bottom, left of two*).—This galaxy is connected to the others through the presence of a very faint R'_1 outer pseudoring of low contrast. This feature is not visible in the Hα or red continuum images but is well illustrated in Figure 23 of the CSRG. The inner regions are defined by a pure spiral of the NGC 5248 type and include four clear spiral arms. These arms are prominent in Hα. The central region is defined mostly by two bright H II regions and diffuse emission (see close-up in Fig. 12). The companion galaxy is ESO 111−9.

ESO 152−26 (Fig. 11, *top*).—The inner ring is very conspicuous in Hα. It includes diffuse emission as well as discrete H II regions. There may be diffuse emission inside the ring. The R_1 component of the outer structure is conspicuous in the continuum image and is clearly dimpled. H II regions line the outer arms and begin close to the bar axis. H II regions near the dimples are not exceptional compared to some away from the dimples. Some H II regions are in one leading quadrant of the R_1 component. There is very bright central emission.

ESO 235−58 (Fig. 11, *middle*).—This was suggested to be a polar ring–related system by Buta & Crocker (1993b), who provide deep blue-light images of the object. The red continuum image shows the probable edge-on central component well. The bulge looks spherical. The central component has elongated diffuse emission centered on the nucleus and is brightest halfway along the disk. The major axis position angle of this emission is slightly different from that of the continuum image. The emission curves into the probable inclined ring component, which has several discrete H II regions. Bright emission comes from the top half of the bulge region, and emission is weak in the dust lane area.

4. PROPERTIES OF THE H II REGIONS

In this section we discuss the properties of the H II regions in the sample galaxies. Luminosity functions, star formation rates, azimuthal variations in emission around rings, and other characteristics are derived to determine how classical ringed galaxies fit into the properties of other galaxies.

4.1. *Finding and Measurement of* H II *Region Fluxes*

Individual H II regions in the sample galaxies were found initially using the DAOFIND routine as incorporated in IRAF. After cleaning the images of residual continuum starlight (due to imperfect subtraction of the brighter local field stars), the images were searched automatically twice, the second time including a small amount of smoothing to increase detection of fainter H II regions. These two lists were merged (after deleting duplicates), and the final list was edited by inspecting the images visually. It is possible to create the entire list visually; however, the two automatic passes reduced the time needed to map a single galaxy.

Hα+[N II] fluxes were measured by integrating the flux within the largest contour which reaches the noise level around a given H II region. For overlapping H II regions, a different procedure was used. In these cases, the IRAF task DAOPHOT was used in group mode to identify members of groups of H II regions. Contour maps of these groups were inspected interactively, and the flux of the whole group within the faintest detectable outer contour was measured. This net flux was then divided among the identified components according to the peak intensity in each. Table 2, column (10), summarizes the number of identified H II regions in each sample galaxy. The numbers range from 40 in the S0$^+$ galaxy NGC 7187 to 977 in the SBb spiral NGC 6300.

4.2. Hα+[N II] *Luminosities*

The Hα+[N II] fluxes of the galaxies were computed in two ways. First, the fluxes of all identified H II regions were summed. This will not in general be equal to the total Hα+[N II] flux of the galaxy because of the presence of diffuse emission and unresolved H II regions. Second, the Hα+[N II] flux was integrated within a circular aperture including the whole apparent emission disk. This estimate includes both resolved and unresolved discrete H II regions as well as diffuse emission.

Table 2, column (2), lists the log of the total integrated Hα+[N II] flux from each galaxy in which a significant flux was measurable. Of the 27 galaxies listed, one, NGC 1832, is in common with the extensive list of Kennicutt & Kent (1983, hereafter KK). Our measured flux, $\log f_{\rm tot} = -11.62$, agrees exactly with that given by KK. However, Kennicutt, Tamblyn, and Congdon (1994, hereafter KTC) note that a scale correction of 1.16 to the fluxes of KK is warranted from a comparison with Romanishin (1990). There are no

TABLE 2

PARAMETERS OF Hα+[N II] DISTRIBUTIONS

Object (1)	log $f_{\rm tot}$ (2)	log $L_{\rm tot}$ (3)	$L_{\rm dis}/L_{\rm tot}$ (4)	log $L_{\rm nuc}$ (5)	SFR (6)	α (7)	σ_α (8)	r(95%) (9)	n (10)	$n_{37.7}$ (11)	$n_{37.7}/L_B$ (12)	Σ (13)
NGC 53	−13.10	40.50	0.79	38.99	0.6	−2.15	0.35	36″.1	66	...	...	...
NGC 210	−11.77	40.93	0.49	39.32:	1.5	−1.86	0.08	137.4	518	195e	102	0.34
NGC 1291[a]	−11.66	40.28	...	...	...	...	...	...	...	...	...	...
NGC 1317	−12.17	40.37	0.72	39.29	0.4	...	...	49.8	44	38:	46	0.73:
NGC 1326	−11.71	40.82	0.48	38.91	1.2	−1.99	0.11	118.2	134	13	9	0.04
NGC 1350	...	...	...	...	...	−1.92	0.16	117.0	161	36	18	0.12
NGC 1433	−11.67	40.54	0.51	39.22	0.6	−1.93	0.05	146.0	779	92	80	0.43
NGC 1832	−11.62	41.30	0.51	39.75	3.6	−2.32	0.20	62.5	206	...	...	...
NGC 6300	−11.22	41.29	0.53	39.78	3.5	−1.87	0.04	113.1	977	453	172	2.35
NGC 6753	−11.69	41.63	0.69	40.04	7.7	−1.65	0.08	63.2	541	...	...	...
NGC 6761	−12.77	41.10	0.12	39.09	2.3	−3.36	0.45	33.9	68	...	...	...
NGC 6782	−12.26	41.25	0.62	39.69	3.2	−1.91	0.10	64.0	296	233e	48	0.32
NGC 6902	−12.15	41.05	0.44	39.21	2.0	−2.33	0.10	130.5	467	371e	79	0.23
NGC 6935	−12.39	41.25	0.46	39.33:	3.2	−2.66	0.19	48.9	315	...	...	...
NGC 6937	−12.14	41.50	0.72	40.68:	4.9	−1.87	0.12	69.5	213	...	...	...
NGC 7020	−12.58	40.66	0.16	39.59:	0.8	−3.04	0.50	84.9	68	41e	22	0.05
NGC 7098	−12.76	40.34	0.76	39.19	0.4	−2.69	0.29	118.5	188	130e	44	0.15
NGC 7187	−13.40	39.74	0.76	38.72	0.1	−1.92	0.33	19.5	40	27	36	0.84
NGC 7219	−12.53	40.65	0.71	39.26	0.8	−1.90	0.17	41.9	139	110e	94	0.67
NGC 7267	−12.32	41.02	0.70	40.36	1.5	−1.80	0.11	47.0	227	122e	57	0.41
NGC 7329	−12.32	40.93	0.40	38.53	1.6	−2.57	0.13	91.2	349	276e	78	0.30
NGC 7531	−11.85	40.81	0.56	38.65	1.2	−1.88	0.07	130.7	549	192	121	0.41
IC 1438	−12.48	40.68	0.67	38.98	0.9	−2.00	0.16	59.7	138	119e	64	0.40
IC 4754	−12.87	40.92	0.44	39.99	1.4	−2.64	0.34	32.2	114	...	...	...
IC 5240	−12.60	40.14	0.41	38.23	0.3	−2.91	0.27	69.4	119	53e	61	0.33
UGC 12646	−12.69	41.49	0.60	41.04	3.7	−1.77	0.26	37.9	63	...	...	...
ESO 111−10.....	−12.82	40.83	0.72	...	1.2	−2.71	0.44	21.7	64	...	...	...
ESO 152−26.....	−12.82	41.03	0.52	40.14	1.7	−3.68	0.38	46.3	236	...	...	...

NOTES.—Col. (1): Object name.
Col. (2): log of total Hα+[N II] emission-line flux (ergs cm^{-2} s^{-1}).
Col. (3): log of total Hα+[N II] luminosity (ergs s^{-1}).
Col. (4): Ratio of Hα+[N II] luminosity in discrete H II regions to total Hα+[N II] luminosity.
Col. (5): log of Hα+[N II] luminosity (ergs s^{-1}) for nucleus only (see text).
Col. (6): Star formation rate ($M_\odot$ yr^{-1}).
Cols. (7), (8): Slope and uncertainty of slope of H II region luminosity function.
Col. (9): Radius which includes 95% of the detected H II regions.
Col. (10): Total number of identified H II regions.
Col. (11): Number of H II regions having L(Hα+[N II]) $> 5 \times 10^{37}$ ergs s^{-1} ("e" means extrapolated using α by no more than 0.2 in the log).
Col. (12): Number of H II regions brighter than 5×10^{37} ergs s^{-1} per unit normalized blue galaxy luminosity (normalization: 10^{10} ergs s^{-1}).
Col. (13): Number of H II regions brighter than 5×10^{37} ergs s^{-1} per unit area (kpc^2) within r(95%).
[a] Includes only the diffuse emission within a circular region of radius 121″.8 centered 11″.0 east, 1″.8 south of the nucleus.

galaxies in our sample in common with Romanishin (1990), and if the KK fluxes are so increased, then our estimate of flux for NGC 1832 is too low by −0.06 dex.

Another external comparison we can make is for the nuclear ring region of NGC 1326. Garcia-Barreto et al. (1991) derived a total Hα flux of 1.38×10^{-12} ergs cm^{-2} s^{-1} for the central 20″ diameter. For the same region, and using the ratio [N II]/Hα = 0.56 derived by Garcia-Barreto et al., our calibration gives an Hα flux of 1.06×10^{-12} ergs cm^{-2} s^{-1}, corresponding to −0.11 dex. Both this and the comparison for NGC 1832 oppose and almost negate the planetary nebula zero point correction we made in section 2.2. Since no such zero-point correction was made in KK, Romanishin (1990), or Garcia-Barreto et al. (1991), the difference may reflect uncertainties in using continuum standards alone.

The luminosities were computed using the distances listed in Table 1, after correction for galactic extinction. The blue-light galactic extinction corrections in RC3 were converted to Hα corrections using the formulation from Cardelli, Clayton, & Mathis (1989). Table 2, column (3), lists the log of the total Hα+[N II] luminosity (called log L_{tot}) in ergs s^{-1}. These luminosities are comparable to those found for galaxies of similar Hubble types by K88, KEH, and Caldwell et al. (1991).

Table 2, column (4), also lists the ratio of the luminosity in discrete H II regions to the total Hα luminosity. KEH derived this ratio for galaxies of different types and found that Sb galaxies tend to have a smaller value of the ratio than Sbc and Sc galaxies. They attributed much of the difference of the ratio from unity to unresolved H II regions below the detection limit. In two Magellanic irregulars, it was found that diffuse interstellar emission contributed to the low ratios observed.

In our ringed galaxy sample, the ratio ranges from 0.12 to 0.76, with an average of 0.56 ± 0.17 (standard deviation). Discrete H II regions therefore account for more than half the Hα luminosity of our sample galaxies. The latest type galaxies in our sample, NGC 210, 1832, 6300, 6753, 6902, 6937, 7219, 7329, and 7531 and ESO 111−10, have a mean ratio of 0.56 ± 0.12 (s.d.). In the early-type galaxies NGC 53, 7098, and 7187, most of the emission is in discrete H II regions. In NGC 6761 and 7020, the ratio is probably low because most of the discrete H II regions are of low luminosity and difficult to identify as such.

4.3. *Luminosity Functions*

The luminosity function of H II regions in each of the sample galaxies was constructed in bins of 0.2 in the log, in order to be directly comparable to the results obtained by KEH. These are shown in Figure 13. Except for a few cases, the luminosity functions display a power-law dependence as seen in other galaxies. The exponent in the function,

$$N(L)dL \propto L^{-\alpha} dL \,, \quad (1)$$

was computed for each galaxy, and the fits are shown in Figure 13. In each case, the points that were used in the fit are shown by filled circles, while those not used are shown by open circles. The drop-off in numbers between 10^{37} and 10^{38} ergs s^{-1} in most of the objects is undoubtedly due to a detection limit, rather than a physical drop-off in the population of H II regions. Most of our galaxies are fairly distant, and we expect not to resolve the fainter H II regions. The resulting exponents are summarized in Table 2, column (7) with errors listed in column (8). The values range from −1.5 to −3.7 and are histogrammed in Figure 14*a*. The mean value, weighted by $1/\sigma_\alpha^2$, is $\langle\alpha\rangle = -1.95 \pm 0.25$ (s.d.), and it is consistent with the means obtained by KEH and Banfi et al. (1993) from different samples of nearby galaxies. KEH have discussed the not-unexpected similarity between H II region luminosity functions with this mean value of α and the luminosity and mass functions of galactic star clusters and molecular clouds.

There are clear effects of prominent nuclear rings in some of the luminosity functions. In NGC 1317, the illustrated luminosity function is dominated entirely by the double nuclear ring and does not follow a power-law function. In NGC 1326 and 6782, the luminosity function shows a change in slope at the highest luminosities due to the bright nuclear ring regions in each case.

One galaxy in our sample, NGC 1832, shows what could be a "type II" differential luminosity function as discussed by KEH. The turnover in the luminosity function for this galaxy occurs precisely at the "critical luminosity" of about 5×10^{38} ergs s^{-1} found by KEH for six galaxies in their sample. A combination of incompleteness and the shallower slope of a type II luminosity function for $L < 5 \times 10^{38}$ ergs s^{-1} could explain the flatter profile below the critical luminosity for this galaxy. None of the other galaxies in our sample show this effect clearly.

4.4. *Other Properties of the* H II *Regions*

Table 2 lists other properties of the H II regions in the sample galaxies. Following KEH, we computed the radius that encloses 95% of the H II regions in each case (called *r*[95%] in col. [9] of Table 2) and the number of H II regions brighter than $L(\text{H}\alpha+[\text{N II}]) = 5 \times 10^{37}$ ergs s^{-1} (called $n_{37.7}$ in col. [11] of Table 2). This number was either counted directly from the compilation of H II regions or obtained by extrapolation of the luminosity function fit if this reached the required level no more than 1 bin (0.2 dex) beyond the last reliable point. These parameters were used to compute the average number density, Σ, of H II regions within the star-forming disk (col. [13] of Table 2), as well as the number of H II regions per unit blue luminosity, $n_{37.7}/L_B$ (col. [12] of Table 2), in each galaxy. These numbers are histogrammed with the same bin size as in KEH in Figures 14*c* and 14*b*, respectively, and they can be compared directly with similar plots in KEH. In many cases, it was not possible to derive these numbers because the value of $n_{37.7}$ required too much extrapolation of the luminosity function. Those values of $n_{37.7}$ requiring a small amount of extrapolation are followed by the letter "e" in Table 2. The numbers in any case are not unusual for the types of the galaxies except for the SBb galaxy NGC 6300, which has more H II regions per unit area than some Magellanic spirals and irregulars. However, NGC 6300 has fewer of the most luminous H II regions ($L \approx 10^{40}$ ergs s^{-1}) than a typical Scd galaxy like M101. It is interesting that in spite of the large number of H II regions associated with the inner ring in NGC 6300, this feature is not prominent in a $B-V$ color index map, suggesting that older stars dominate even the blue-light appearance (Buta 1987b).

4.5. *Star Formation Rates*

The star formation rates in our sample galaxies were computed using the method outlined by Kennicutt (1983, here-

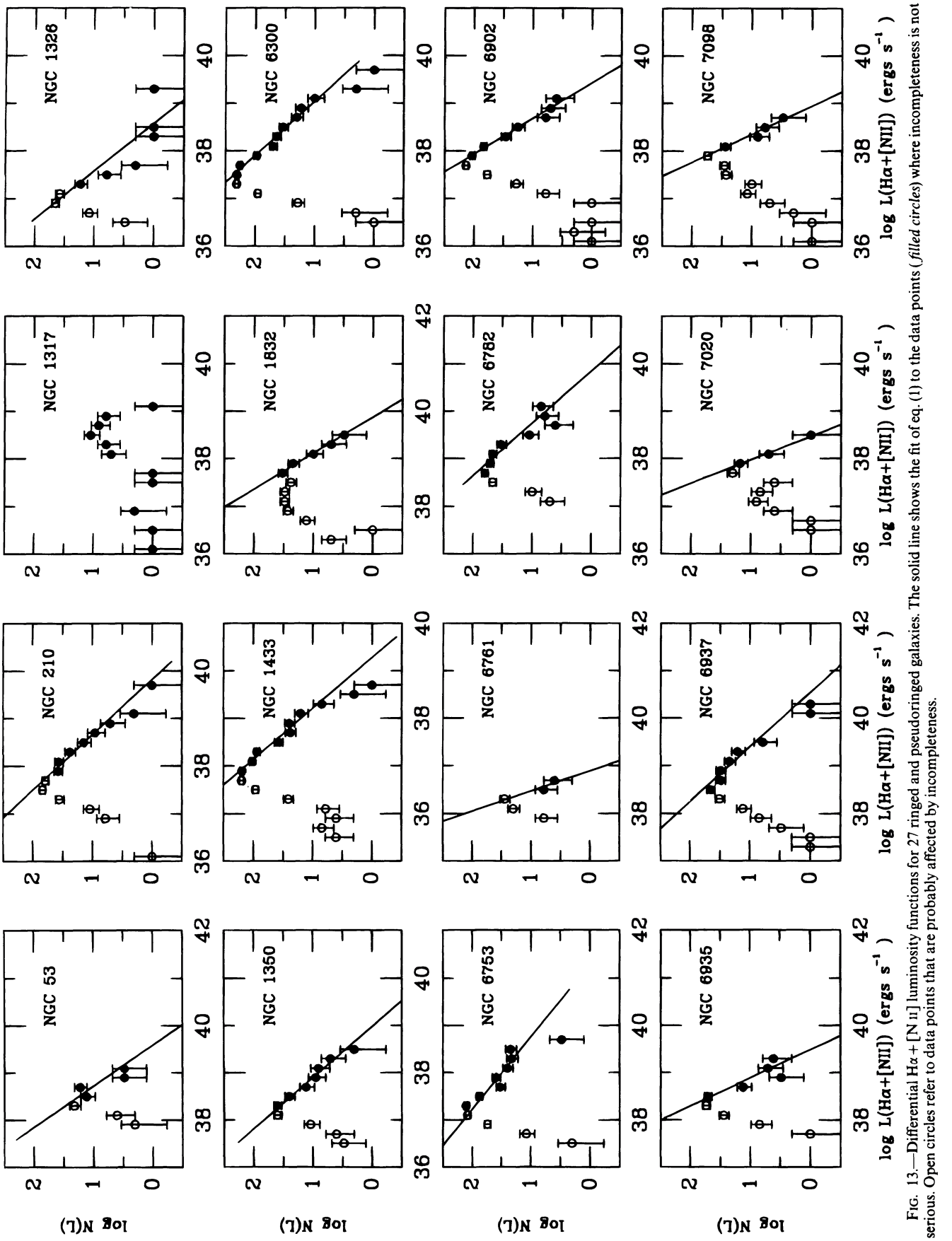

FIG. 13.—Differential Hα + [N II] luminosity functions for 27 ringed and pseudoringed galaxies. The solid line shows the fit of eq. (1) to the data points (*filled circles*) where incompleteness is not serious. Open circles refer to data points that are probably affected by incompleteness.

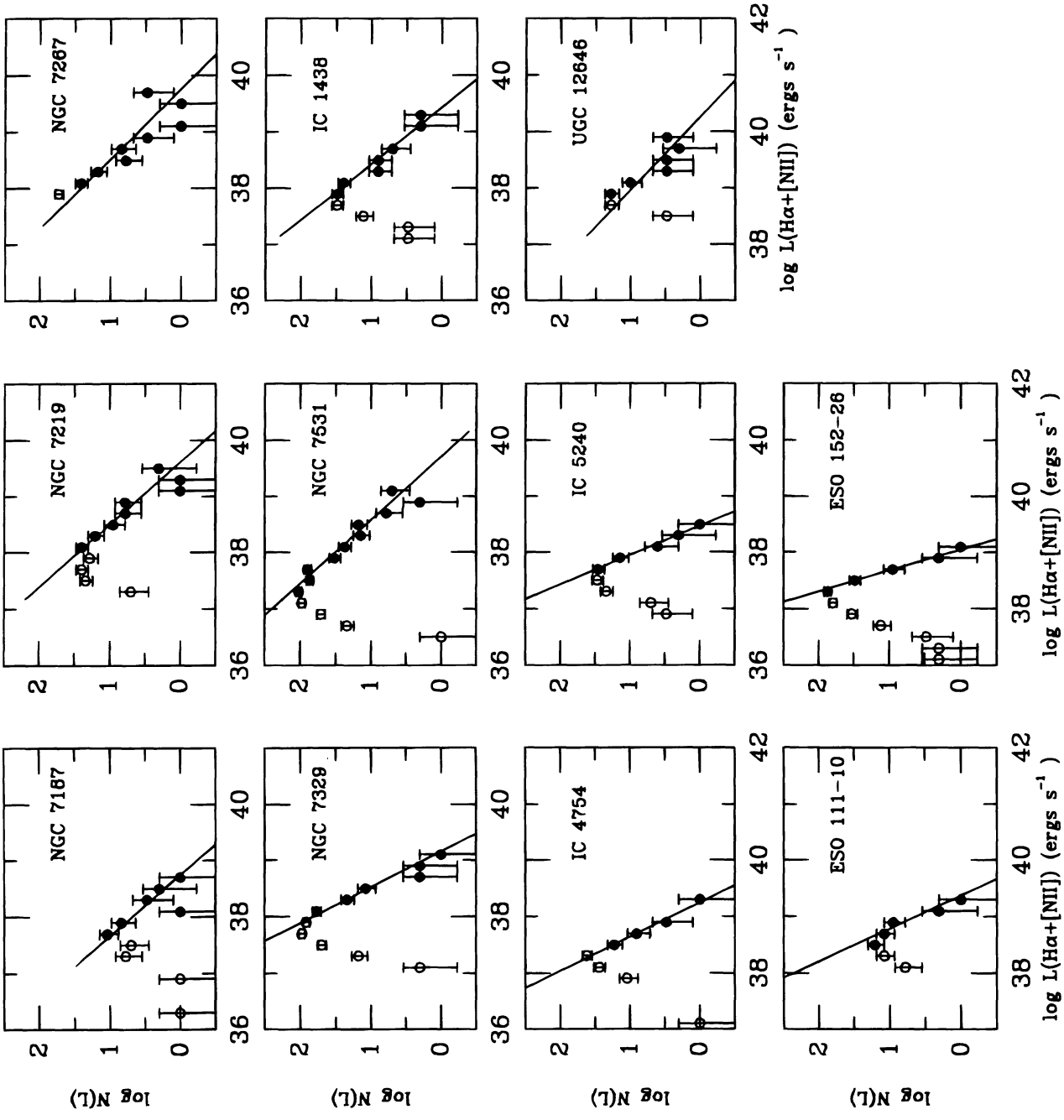

FIG. 13.—*Continued*

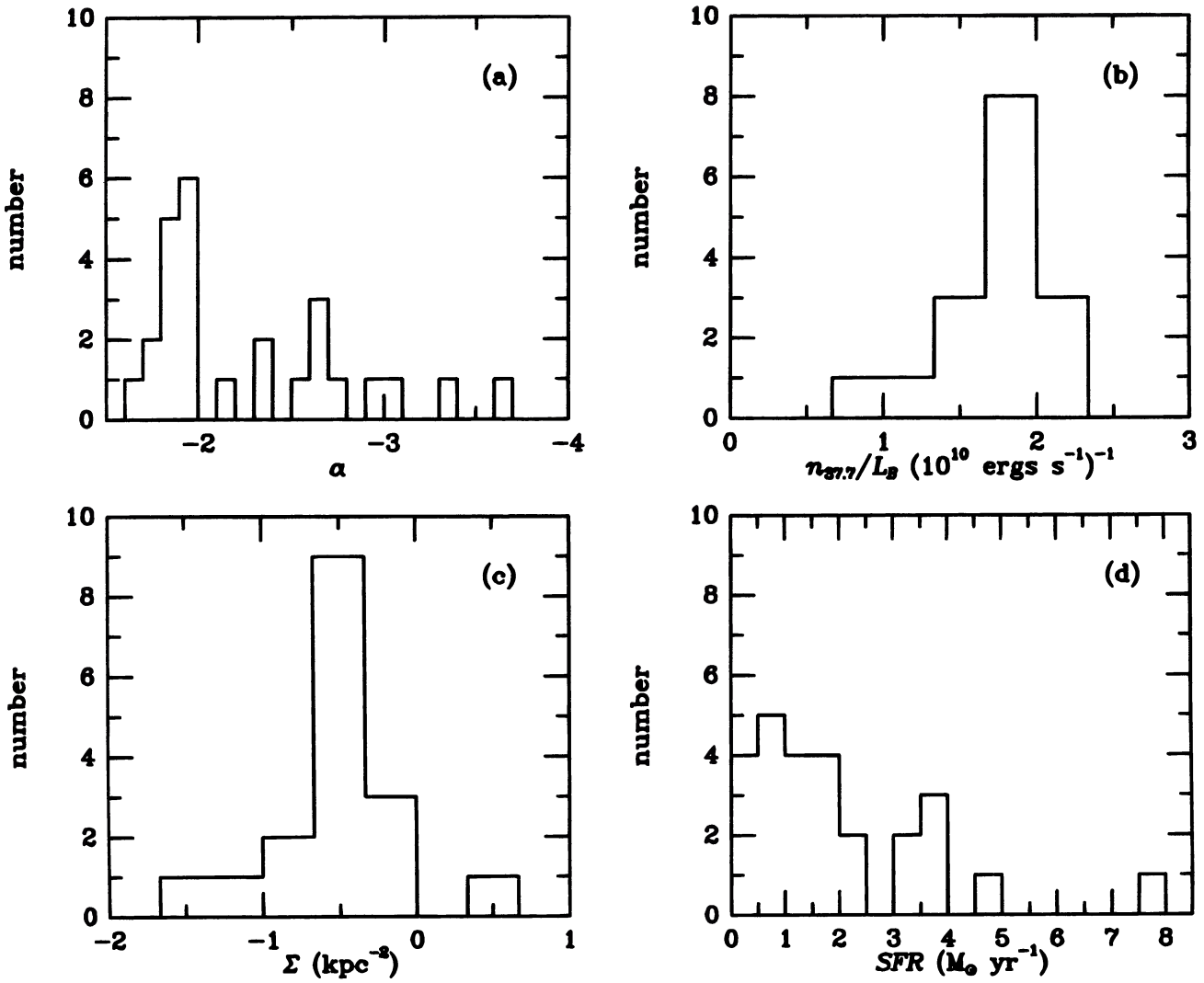

FIG. 14.—Histograms of derived properties of H II region distributions in sample galaxies: (*a*) distribution of power-law indices α in eq. (1); (*b*) distribution of number of H II regions having $L(\mathrm{H}\alpha+[\mathrm{N\ II}]) > 5 \times 10^{37}$ ergs s^{-1} per unit blue galaxy luminosity; (*c*) distribution of same number of H II regions per unit area within the disk that encloses 95% of the total number of detected H II regions; and (*d*) distribution of the total star formation rate computed from the corrected Hα luminosity.

after K83).[4] These rates are derived from the total Hα luminosity under the assumption of case B recombination theory and a standard initial mass function. Following K83, we assume that the contribution of Hα alone is 75% of our measured Hα+[N II] luminosities and that the average internal extinction at Hα is 1.1 mag. We also subtracted off the nuclear emission from each total luminosity to minimize the effects of any nuclear activity; these nuclear luminosities are given in column (5) of Table 2. The star formation rates derived are listed as SFR in column (6) of Table 2 and are histogrammed in Figure 14*d*. The rates range from 0.1 $M_\odot$ yr^{-1} for the S0$^+$ galaxy NGC 7187 to 7.7 $M_\odot$ yr^{-1} for the Sb galaxy NGC 6753. These rates cannot be compared directly to those given in K83, who used a distance scale based on $H_0 = 50$ rather than 75 as used here. However, when taking this into account they are consistent with K83.

Several of the early types (notably NGC 1317, 1326, and 6782) have star formation rates influenced by their bright nuclear rings. To examine how much these small rings contribute, we have isolated the emission from the nuclear ring regions in five galaxies in Table 3. In each case, the "nuclear ring region" was defined to be a region extending from near the nucleus to just beyond the ridge line of the feature. The radius ranges are listed in column (3) of Table 3. The ridge lines of the rings were mapped visually using a cursor on a TV monitor, and the points were fitted with an ellipse. The parameters of these fitted ellipses are given in columns (6)–(8) of Table 3. The ridge lines of both nuclear rings of NGC 1317 were fitted separately and are listed separately in Table 3. In addition, we can define two partial nuclear rings in NGC 1433, the parameters of which are also given in Table 3. The nuclear ring orientations for NGC 1317 can be compared with the position angles of the prominent nuclear

[4] KTC use an improved stellar library and several different initial mass functions (IMFs) from K83. For the same IMF as used by K83, they derived star formation rates about 20% lower than would be given by the K83 analysis.

TABLE 3

PARAMETERS FOR NUCLEAR RINGS

Object (1)	log L_{nr} (2)	Range (3)	L_{nr}/L_{tot} (4)	SFR_{nr} (5)	a_{nr} (6)	q_{nr} (7)	ϕ_{nr} (8)
NGC 1317	40.29	2″.8–19″.5	0.83	0.4	12″.5[a]	0.79[a]	52°[a]
					14.9[b]	0.89[b]	157[b]
NGC 1326	40.74	1.3–13.0	0.83	1.0	5.7	0.71	85
NGC 1433[c].....	39.69	2.0–13.0	0.14	0.1	7.4[a]	0.85[a]	20[a]
					10.9[b]	0.86[b]	10[b]
NGC 6782	40.91	1.5–8.7	0.46	1.5	4.6	0.94	111
IC 1438	40.07	1.1–6.5	0.25	0.2	3.5	0.77	80

NOTES.—Col. (1): Object name.

Col. (2): log of Hα + [N II] lumiosity (ergs s^{-1}) from nuclear ring region as defined in col. (3).

Col. (3): Radius range used for integrating flux of nuclear ring.

Col. (4): Relative contribution of nuclear ring to total Hα + [N II] luminosity.

Col. (5): Star formation rate for defined nuclear ring region ($M_\odot$ yr^{-1}).

Cols. (6)–(8): Major axis radius, axis ratio, and major axis position angle of nuclear ring as defined by ridge line in emission.

[a] Inner nuclear ring of double feature.

[b] Outer nuclear ring of double feature.

[c] Both features are partial rings.

bar ($\phi = 57°$) and the primary oval ($\phi = 150°$). The nuclear bar is closely aligned with the inner nuclear ring, while the primary oval is closely aligned with the outer nuclear ring.

The contribution of each nuclear ring region to the total Hα + [N II] luminosity is listed in column (4) of Table 3. In NGC 1317 and 1326, the nuclear ring zones as defined contribute 83% of the total Hα + [N II] luminosity. Those in NGC 1433, NGC 6782, and IC 1438 contribute considerably less to the total luminosity. The star formation rates from these zones range from 0.1 to 1.5 $M_\odot$ yr^{-1}.

4.6. *Distribution of* H II *Regions around Inner Rings*

As described in § 1, one possible way of connecting the distribution of H II regions in ringed galaxies to internal dynamics is to examine the distribution of H II regions around inner rings. We expect that in the most intrinsically oval inner rings, the H II regions will concentrate around the inner ring major axis because that is where the gas would move slowest. Our sample includes rings with a wide range of intrinsic axis ratios, and thus we can investigate this question reliably. For this part of our study, we were able to add an extra galaxy to the sample: NGC 3081. This object was observed at Hα with a Fabry-Perot interferometer in 1992 by G. B. Purcell and R. Buta. The details of these observations will be presented elsewhere, but here we use the distribution of Hα emission in the bright inner ring given by the interferometry to increase the number of intrinsically oval rings in our sample.

The procedure was as follows. First, the orientation parameters of the galaxy and the position angle of the bar were estimated by fitting ellipses to isophotes in the continuum image. The orientation parameters were defined by the faintest surface brightness level that gave a coherent isophote. These orientation parameters (listed in Table 4) were then used to deproject the H II region positions and the bar position angle. Next, each inner ring was mapped visually in the red continuum image using a cursor on a TV display. These points were then deprojected and fitted with an ellipse, which was used to locate H II regions associated with the ring within a specified range in radius. This procedure was used instead of starting directly with the H II regions because of the problem of biasing due to extra H II regions from the outer arms at the ends of the bar. Such a bias would enhance the effect we are searching for. Once a ring was isolated, the Hα + [N II] fluxes were computed as a function of position angle θ relative to the line of nodes in the galaxy plane.

TABLE 4

ADOPTED ORIENTATION PARAMETERS

Object (1)	ϕ_G (2)	q_G (3)	ϕ_B (4)
NGC 53	148	0.80	174
NGC 210	159	0.69	171
NGC 1326.....	75	0.75	18
NGC 1350.....	3	0.55	37
NGC 1433[a].....	17	0.85	96
NGC 1832.....	1	0.69	168
NGC 3081.....	89	0.85	66
NGC 6300.....	105	0.66	76
NGC 6753.....	35	0.85	...
NGC 6761.....	80	0.93	3
NGC 6782.....	35	0.89	177
NGC 6902.....	131	0.80	129
NGC 6935.....	9	0.95	...
NGC 6937.....	28	0.78	160
NGC 7020.....	163	0.44	165
NGC 7098.....	71	0.58	49
NGC 7187.....	140	0.90	...
NGC 7219.....	30	0.64	...
NGC 7267.....	3	0.90	106
NGC 7329.....	112	0.70	76
NGC 7531.....	20	0.45	13
IC 1438	145	0.90	123
IC 4754	115	0.89	11
IC 5240	100	0.69	92
UGC 12646	38	0.90	137
ESO 111−10.....	115	0.62	102
ESO 152−26.....	20	0.65	146

NOTES.—Col. (1): Object name.

Cols. (2), (3): Position angle and axis ratio of galaxy disk, based on fitting of an ellipse to the faintest reliable continuum isophote.

Col. (4): Bar position angle, based on fitting of an ellipse.

[a] Object overflowed CCD field; parameters from Buta 1986 adopted.

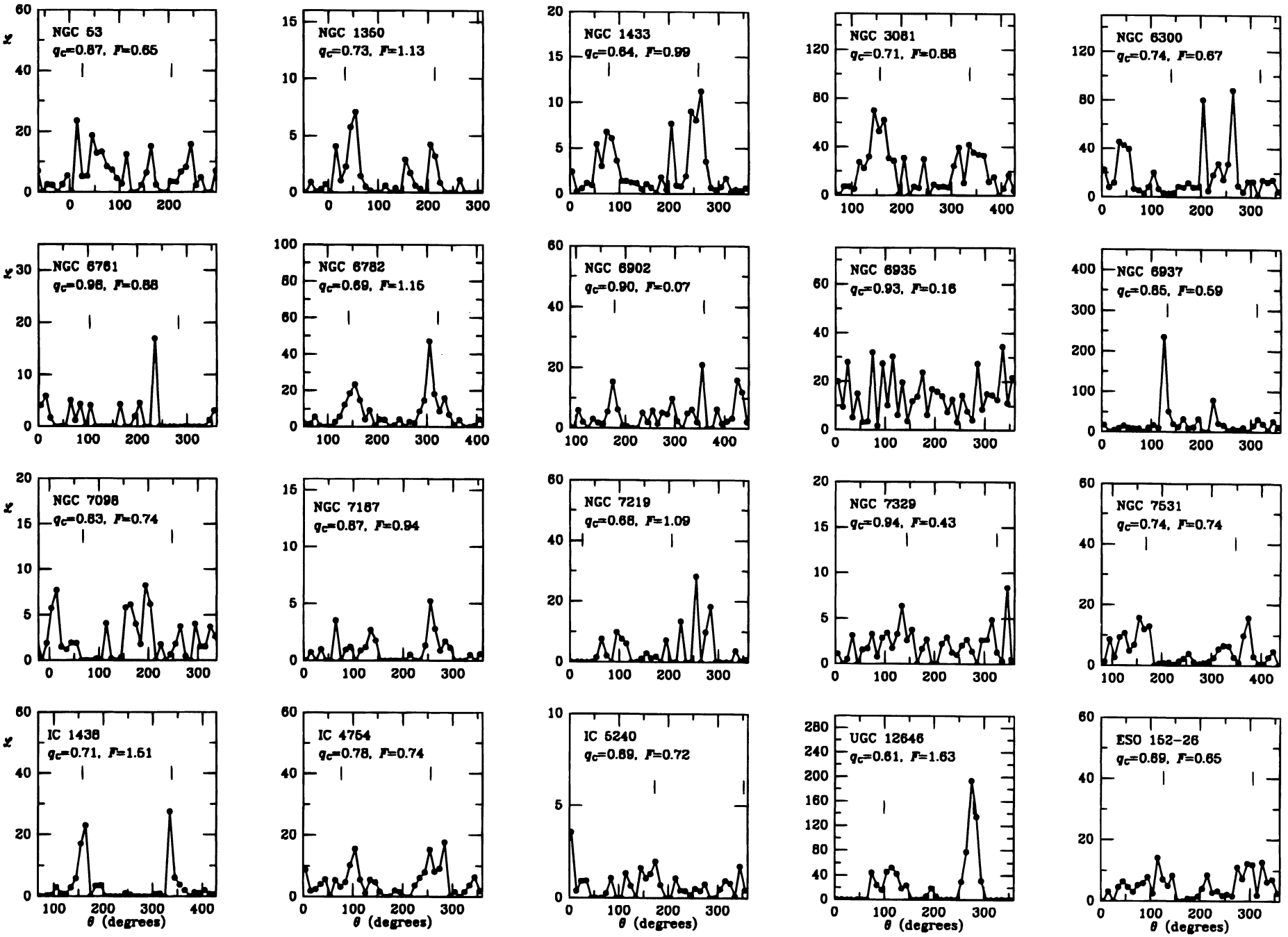

FIG. 15.—Luminosity/position angle diagrams for the inner rings in 20 galaxies. The ordinate is the normalized luminosity $\mathscr{L} = L(\mathrm{H}\alpha + [\mathrm{N\ II}])/10^{38}$, while the abscissa is the angle in the galaxy plane relative to the adopted line of nodes (Table 4). Each panel gives the name of the galaxy, the deprojected axis ratio, q_C, of the inner ring as deduced from a visual mapping of the feature on the continuum image, and the relative 2θ Fourier amplitude F (see text). The data for NGC 3081 are based on uncalibrated Fabry-Perot interferometer images. The short vertical lines refer to the ends of a bar when present.

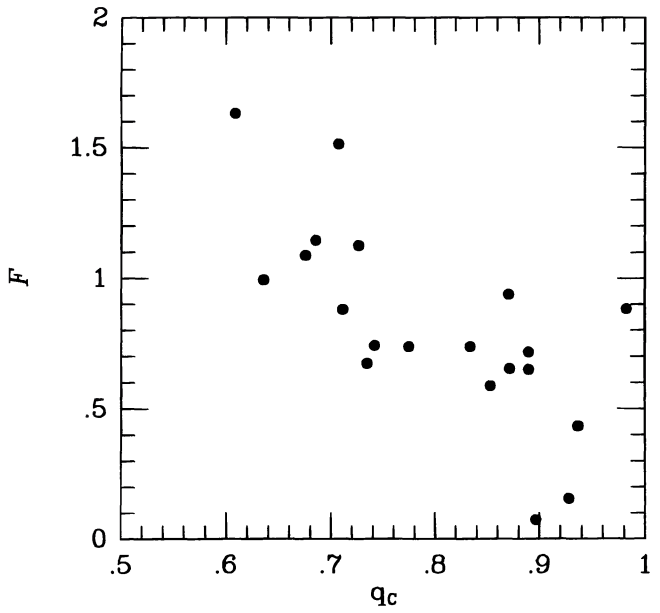

FIG. 16.—Plot of the relative 2θ Fourier amplitude, F, vs. the deprojected continuum axis ratio, q_C, of the inner ring.

The resulting luminosity/position angle diagrams for 20 inner rings are shown in Figure 15. In each panel, the deprojected continuum axis ratio, q_C, is indicated and the two vertical dashes indicate the approximate deprojected bar position angle if a bar exists. The plots definitely show a characteristic pattern in the distribution of emission from discrete H II regions around the most oval inner rings. NGC 6782, IC 1438, and UGC 12646 show most of their emission near the ring major axis and very little emission near the ring minor axis. The same is true for NGC 1433 and NGC 3081, but there is more emission near the minor axes in those cases. In contrast, the nearly circular rings in NGC 53, NGC 6902, NGC 6935, and NGC 7329 show a more random distribution of emission with azimuth around the rings. This suggests that intrinsic shape does affect the way H II regions are distributed around a ring. To quantify this effect, we have analyzed the luminosity/position angle diagrams via Fourier analysis and computed the relative amplitude, $F = I_2/I_0$, where I_2 is the amplitude of the 2θ component of the luminosity distribution and I_0 is the mean luminosity around the ring. The values of F for each galaxy are given in Figure 15 and are plotted versus continuum ring axis ratio q_C in Figure 16. A definite correlation is in evidence. Those rings with $q_C \leq 0.72$ tend to have $F \geq 0.9$, while those rings with $q_C > 0.8$ tend to have $F < 0.9$. The scatter is large, probably for a variety of reasons: (1) If few H II regions are detected in a ring, the amplitude can be affected by small number statistics. This problem is most serious for NGC 6761 in our sample. (2) The flux limit may cause faint H II regions in the rings to be undetected. Since this affects H II regions in all parts of the ring, not just the major or minor axes, it is probable that the 2θ amplitude is not seriously over- or underestimated by their absence, unless the slope of the luminosity function of H II regions depends on azimuth around the ring. (3) Accurate deprojection of the rings is not really possible because assumptions have to be made concerning the shape of the outer disk. The continuum axis ratio q_C is based on a visual mapping and this uncertain deprojection, and hence it can be in error as a result. We anticipate errors of at least ± 0.05 for q_C. (4) In addition to the effect of the shape of the ring, there is also probably still some randomness regarding where an H II region may form in a ring. Thus, even the most oval inner rings can still have a bright H II region near the ring minor axis as, for example, in UGC 12646 and NGC 1433.

A clue to the nature of this effect is provided by how well the bar axis agrees with the phase of the maxima in the (luminosity position angle) diagram. In NGC 1350, 1433, 3081, and 6782, IC 1438, and UGC 12646, the bar axis coincides with the maxima. We believe that this implies that the inner rings of these galaxies lie *within* and probably close to the corotation resonance (CR). According to Contopoulos (1979), a particle within CR would stay longer at the apocentra of its orbit than the pericentra, which would enhance the density along the major axis of all orbits within CR. Adding to this enhancement inside CR is that the elongation of the orbits brings matter from the inner, denser regions to the major axis of the orbits. Working against these two effects is orbit crowding just inside CR, which tends to be maximum near the minor axis of the orbits. However, since we have found no clearly aligned inner rings where the ring *minor axis* is enhanced relative to the ring major axis, we believe that this effect is not generally important in the most elongated inner rings. The suggestion by Schwarz (1984) that inner rings are connected to the inner 4:1 resonance located just inside CR is supported by our findings.

There are some clear cases of misalignment between bars and the H II region concentration peaks in a few inner rings. The strongest case is NGC 6300, in which the H II region peaks are about 90° away from the bar axis. The misalignment in NGC 6300 has been noted previously by Buta (1987b), and it may be a case in which the bar and spiral pseudoring are independent patterns (Sygnet et al. 1988). IC 4754 is another case listed as a suspected misaligned bar/ring galaxy in Table 4 of the CSRG. Misaligned bar/ring galaxies are discussed further by Crocker, Muzerolle, & Buta (1992) and Buta, Purcell, & Crocker (1995).

5. DISCUSSION

We have shown that the distribution of H II regions in early-to-intermediate Hubble type ringed galaxies has a great deal of variety. In NGC 53, 1433, 6300, 6935, and 7187, most of the H II regions are concentrated in an inner ring, while in NGC 1317 they are concentrated in a double nuclear ring. The inner ring of NGC 1326 is notably devoid of H II regions. In other galaxies we see H II regions connected to spiral structure and to all three ring and pseudoring types, if present. In NGC 1317 and 1326, more than 80% of the total Hα+[N II] luminosity comes from the nuclear ring regions. As noted by Ryder & Dopita (1993), the bar regions of these early-type systems tend to be deficient in H II regions, especially when the inner rings include many H II regions. The galaxy NGC 7267, classified as having an R'_1 outer pseudoring in the CSRG, is an exception which has a bar rich in Hα emission but no ringlike patterns of H II regions.

Our original goal of trying to tie the distribution of H II regions in ringed galaxies to the properties of resonant periodic orbits in a bar potential appears at first sight to have been successful. Extremely oval inner rings show a

greater concentration of H II regions and Hα luminosity near the intrinsic ring major axis compared to the intrinsic ring minor axis. We do not believe that this is an artifact of extinction. Can we see evidence of similar orbit characteristics for nuclear and outer rings and pseudorings among the galaxies of our sample?

The double nuclear ring in NGC 1317 shows characteristics consistent with an interpretation in terms of an inner Lindblad resonance (ILR). The inner nuclear ring is aligned nearly perpendicular to the primary bar/oval and may be connected to the x_2 family of periodic orbits. In this circumstance, it would have to lie between two ILRs or inside a single ILR. The outer nuclear ring is nearly aligned parallel to the primary bar/oval, and it may be connected to periodic orbits of the x_1 family located just outside the outer ILR of a double ILR. According to Contopoulos (1979), orbit crowding and elongation would enhance the density along the major axis just outside the outer ILR, while orbit crowding would not enhance the major axis density between the two ILRs. Neither nuclear ring in NGC 1317 shows much variation in the Hα luminosity and H II region density with azimuth that might be connected to these effects. The rather round shapes of both features and the fact that they nearly intersect may minimize the expected effects.

The nuclear bar of NGC 1317 is oriented almost exactly perpendicular to the primary bar/oval, as noted many years ago by Schweizer (1980). As shown by Buta & Crocker (1993a) and Wozniak et al. (1995), nuclear bars can have any angle relative to the primary bar; this is possibly due to different pattern speeds. Thus it is, intriguing and perhaps coincidental that the bar and nuclear rings of NGC 1317 have alignments with respect to the primary bar/oval that are so close to those expected from periodic orbit theory. Is this a case in which the nuclear and primary bars do have the same pattern speed?

The characteristics of outer rings and pseudorings in our sample galaxies are quite varied. The outer ring of NGC 7020, and the outer pseudorings of NGC 210, 6753, 7098, 7219, and 7417, IC 1438, and ESO 152−26 are rich in H II regions, while the outer rings of NGC 6932, 7187, and 7702, and the outer pseudorings of NGC 53, 1317, 1350, 1433, and 7267, are not well defined as ring or pseudoring patterns in Hα. One of the most important findings we have made about outer rings is how the distribution of H II regions in some galaxies with prominent R_1 or R_1' outer rings follows an R_2' shape. This is seen in NGC 1326, NGC 6782, IC 1438, and UGC 12646, and we believe the dichotomy may be connected to secular evolution of the gas distribution as illustrated by test-particle models in Byrd et al. (1994). When a bar is turned on in the axisymmetric potential of a stellar disk, gas clouds initially distributed in circular orbits are forced into the periodic orbits of the bar field and collide near resonances with the bar pattern speed. Byrd et al. show that a pseudoring develops near the outer Lindblad resonance (OLR) that initially has the R_1' shape. However, after a number of bar rotations, this shape disappears and is replaced by an R_2' shape. If the R_1' phase can last long enough, it may leave behind a stellar remnant, and indeed we note that in all four of the above galaxies, an R_1 or R_1' component is the main outer feature seen in the continuum images. Thus, we speculate that in these galaxies, the gas distribution has evolved beyond the R_1' phase into the R_2' phase. We note also that all four of these galaxies have bright strings of H II regions in the trailing quadrants of the R_1 component, which is consistent with expectations from the test-particle models (see Fig. 3b of Byrd et al. 1994, and refer to the 3.5 bar rotation frame of the pattern speed 0.06 simulations).

In NGC 1433 and 1350, we see that the H II regions beyond the inner rings are concentrated mainly in arcs around or leading the bar axis. In each case, the major axis of the outer pseudoring has very few H II regions, and the ring is not prominent as such in Hα. The secondary arcs in NGC 1433 are undoubtedly connected to a general four-armed pattern which may be expected around corotation under certain conditions (see Fig. 12*b* of Byrd et al. 1994).

One aspect of outer rings that is not well illustrated with the sample here is the occurrence of bright H II regions near "dimples" in an R_1 outer ring or R_1' outer pseudoring. Weak dimpling is often seen in blue-light images of such rings and is thought to reflect the character of one of the main families of periodic orbits expected near the OLR. In the sample here, the southern dimple of NGC 1326 shows a bright H II region, and nonexceptional H II regions are also seen at dimple points in the R_1' components of NGC 7098 and ESO 152−26. However, we have found another galaxy, IC 4214, in which the brightest H II regions in the galaxy are located at oppositely positioned dimple points (Buta, Lewis, & Purcell 1995). The dimple points are where gas in the inner OLR orbit family is expected to move slowest in the bar frame (Contopoulos 1979), and perhaps we might expect such regions to produce bright H II regions. Nevertheless, strong blue-light dimpling, as in UGC 12646, apparently does not guarantee the existence of such H II regions. Further studies of the kinematics of these galaxies should help to elucidate how material is moving in the dimple regions.

Perhaps the most unusual case in our sample is NGC 1291. The optical properties of this nearby outer-ringed galaxy were derived by de Vaucouleurs (1975), who discovered a secondary bar within the bulge and incipient resolution in the outer ring. As we have noted, the ionized gas distribution in the region of the primary bar, inner lens, and bulge appears uncorrelated with the optical morphology. The shape and orientation of this region differs considerably from that of the oval lens and bar. The diffuse ionized gas is entirely confined to the well-known H I hole in this galaxy (van Driel, Rots, & van Woerden 1988), and the wispy structure is very reminiscent of what is seen in the bulge region of the Andromeda galaxy. Ciardullo et al. (1988) present very detailed Hα+[N II] images of M31 that reveal an extremely complex pattern of diffuse emission, part of which may be more face-on than the main stellar disk of the galaxy. Since NGC 1291 is thought to be inclined by as little as 6° (Mebold et al. 1979), we have investigated how isophotes of the diffuse Hα+[N II] emission compare quantitatively with isophotes of the continuum starlight. Figures 17*a* and 17*b* show the results of ellipse fits to the data to radii just beyond the prominent inner lens. Although ellipses fit the continuum light well, except in the bar regions, isophotes of the diffuse emission are very irregular and not so well represented. In spite of this, Figure 17*a* shows that the ellipse fit surface brightness profiles of the starlight and the ionized gas are remarkably similar in this galaxy. The similar surface brightness profiles show that on average the ionized gas feels the potential of the stars. Details of the gas distribution are chaotic, however, and misalignments are present. Without kine-

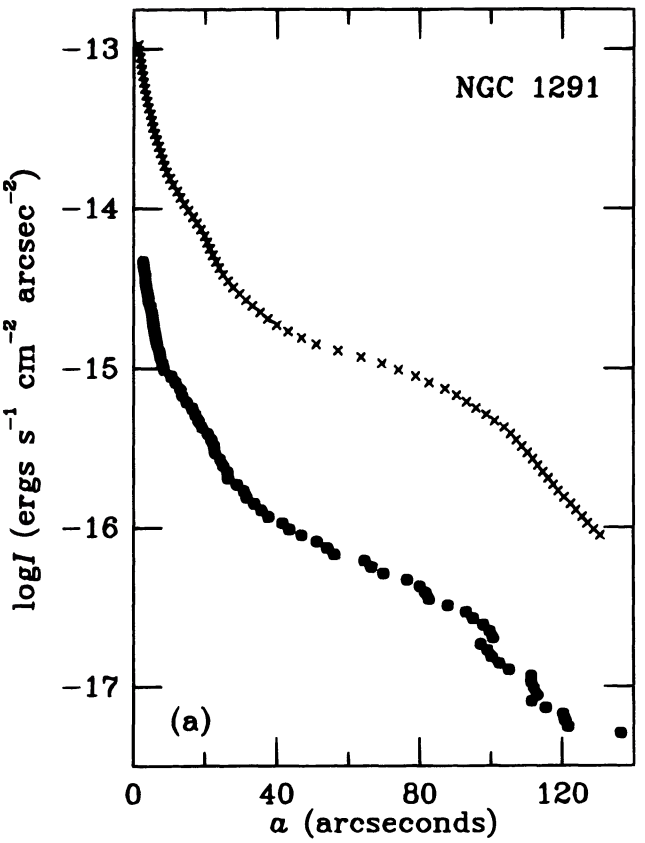

FIG. 17a

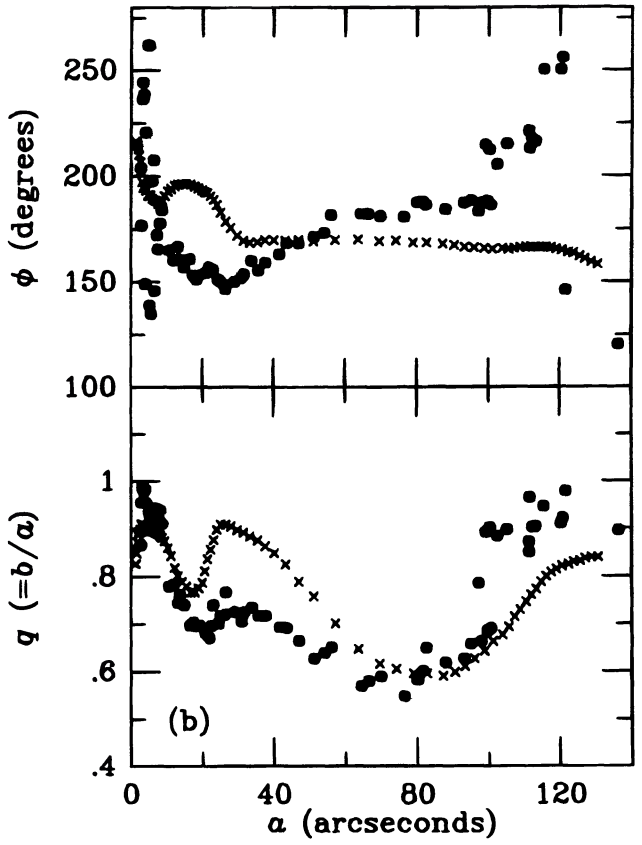

FIG. 17b

FIG. 17.—Results of ellipse fits to continuum and emission-line data for NGC 1291: (*a*) surface brightness profiles; (*b*) axis ratio and position angle profiles. Crosses refer to the continuum data, and filled circles refer to the Hα+[N II] data.

matic data we cannot say whether the gas is in the same plane as the stellar disk of NGC 1291.

Jacoby, Ford, & Ciardullo (1985, hereafter JFC) have calculated the mass of ionized gas in a region of projected area 760 × 760 pc in the bulge of M31. Only 1500 $M_\odot$ of such gas is present and attributed to mass loss from evolving low-mass stars. In NGC 1291, we observe the wispy diffuse ionized gas to a radius of at least 122″ or 5.1 kpc and find a total Hα+[N II] luminosity of 1.9×10^{40} ergs s^{-1} (Table 2). We do not know the electron density over this large region, but to compare with M31 we can compute the ionized gas mass within the half-light radius (29″ = 1.2 kpc) of this emission. By assuming similar properties of the gas (electron density 10^3 cm^{-3}, [N II]/Hα flux ratio of 2.6, emitting gas confined to 200 pc thickness) as JFC used for M31, and using equations provided by Peimbert (1968), we estimate a mass in ionized gas of $\approx$6000 $M_\odot$ in this region of NGC 1291. This would be an underestimate owing to the slight core saturation.

To account for the small amount of ionized gas mass in the bulge of M31, Ciardullo et al. (1988) suggested that much of the interstellar medium produced by the evolution of the stars in the bulge is ejected via a galactic wind fueled by supernova explosions. This may also be a reasonable explanation for what we seen in NGC 1291. Recently, Bregman, Hogg, & Roberts (1995) have shown that the H I hole in NGC 1291 is occupied by hot X-ray–emitting gas. The radial surface mass density of this hot gas has a profile that strongly resembles the profiles in Figure 17*a*. Both a soft and a hard X-ray component to the surface brightness distribution were found. The soft component could be due mainly to gas from stellar mass loss.

6. CONCLUSIONS

We have presented a CCD atlas of the distribution of H II regions in 32 ringed and pseudoringed galaxies covering a range of ring and Hubble types. We have found evidence that the distribution of H II regions in these kinds of galaxies is connected to the properties of the main periodic orbits in the gravitational potential of a bar or barlike perturbation. The results support the idea that ring and pseudoring phenomena are connected to specific orbital resonances with the bar. Most interesting is the variation in Hα properties that we find for these kinds of galaxies. It is likely that these variations are connected not only to internal dynamics, but also to differences in gas content, mass distribution, and evolutionary state between the galaxies. The imaging and analysis of many more examples will undoubtedly shed more light on the structure and dynamics of these kinds of galaxies.

We thank Guy B. Purcell and Lauren V. Jones for their assistance in obtaining the images used in this paper. We also thank the staff at CTIO for the efficient and smooth operation of the instrumentation. This work was supported in part by NSF grant AST 9014137, NSF REU grant AST 9300413, and NSF EPSCoR grant EHR-9108761 to the University of Alabama.

REFERENCES

Aaronson, M., Huchra, J., Mould, J., Schechter, P., & Tully, R. B. 1982, ApJ, 258, 64
Banfi, M., Rampazzo, R., Chincarini, G., & Henry, R. B. C. 1993, A&A, 280, 373
Bregman, J., Hogg, D. E., & Roberts, M. S. 1995, ApJ, 441, 561
Buta, R. 1986, ApJS, 61, 631
———. 1987a, ApJS, 64, 1
———. 1987b, ApJS, 64, 383
———. 1990a, ApJ, 354, 428
———. 1990b, ApJ, 356, 87
———. 1991, ApJ, 370, 130
———. 1995, ApJS, 96, 39 (CSRG)
Buta, R., & Crocker, D. A. 1991, AJ, 102, 1715
———. 1993a, AJ, 105, 1344
———. 1993b, AJ, 106, 939
Buta, R., Lewis, M., & Purcell, G. B. 1995, in preparation
Buta, R., Purcell, G. B., & Crocker, D. A. 1995, AJ, 110, 1588
Byrd, G., Rautiainen, P., Salo, H., Buta, R., & Crocker, D. A. 1994, AJ, 108, 476
Caldwell, N., Kennicutt, R., Phillips, A. C., & Schommer, R. A. 1991, ApJ, 370, 526
Cardelli, J., Clayton, G. C., & Mathis, J. S. 1989, ApJ, 345, 245
Ciardullo, R., Rubin, V. C., Jacoby, G. H., Ford, H. C., & Ford, W. K. 1988, AJ, 95, 438
Contopoulos, G. 1979, in Photometry, Kinematics, and Dynamics of Galaxies, ed. D. S. Evans (Austin: Univ. of Texas Dept. of Astronomy), 425
Crocker, D. A., Muzerolle, J., & Buta, R. 1992, BAAS, 24, 1123
de Vaucouleurs, G. 1959, Handbuch der Physik, 53, 275
———. 1975, ApJS, 29, 193
de Vaucouleurs, G., de Vaucouleurs, A., Corwin, H. G., Buta, R., Paturel, G., & Fouqué, P. 1991, Third Reference Catalogue of Bright Galaxies (New York: Springer)
Gallagher, J., & Hunter, D. A. 1984, ARA&A, 22, 37
García-Barreto, J. A., Dettmar, R.-J., Combes, F., Gerin, M., & Koribalski, B. 1991, Rev. Mexicana Astron. Astrofis., 22, 197
Jacoby, G. H., Ford, H. C., & Ciardullo, R. 1985, ApJ, 290, 136 (JFC)
Jacoby, G. H., Quigley, R. J., & Africano, J. L. 1987, PASP, 99, 672
Kennicutt, R. C. 1983, ApJ, 272, 54 (K83)
———. 1988, ApJ, 334, 144 (K88)
Kennicutt, R. C., Edgar, B. K., & Hodge, P. W. 1989, ApJ, 337, 761 (KEH)
Kennicutt, R. C., & Kent, S. M. 1983, AJ, 88, 1094 (KK)
Kennicutt, R. C., Tamblyn, P., & Congdon, C. W. 1994, ApJ, 435, 22 (KTC)
Kohoutek, L., & Martin, W. 1981, A&AS, 44, 325
Mebold, U., Goss, W. M., van Woerden, H., Hawarden, T. G., & Siegman, B. 1979, A&A, 74, 100
Peimbert, M. 1968, ApJ, 154, 33
Pogge, R., & Eskridge, P. 1993, AJ, 106, 1405
Romanishin, W. 1990, AJ, 100, 373
Ryder, S., & Dopita, M. A. 1993, ApJS, 88, 415
Sandage, A. 1961, The Hubble Atlas of Galaxies (Carnegie Institution of Washington Publ. No. 618)
Sandage, A., & Bedke, J. 1994, The Carnegie Atlas of Galaxies (Carnegie Institution of Washington Publ. No. 638)
Schwarz, M. P. 1984, MNRAS, 209, 93
Schweizer, F. 1980, ApJ, 237, 303
Sygnet, J. F., Tagger, M., Athanassoula, E., & Pellat, R. 1988, MNRAS, 232, 733
Tully, R. B. 1988, Nearby Galaxies Catalog (Cambridge: Cambridge Univ. Press)
van Driel, W., Rots, A., & van Woerden, H. 1988, A&A, 204, 39
Wozniak, H., Friedli, D., Martinet, L., Martin, P., & Bratschi, P. 1995, A&AS, 111, 115

Note added in proof.—In a detailed comparison of nuclear, disk, and "hot-spot" H II regions in several galaxies, Kennicutt, Keel, & Blaha (AJ, 97, 1022 [1989]) found that nuclear ring hot-spot H II regions tend to have luminosities similar to disk H II regions, in spite of the fact that the hot spots look brighter in a visual inspection of images. Our results concur with theirs, except for NGC 1326 and NGC 6782, where the nuclear ring H II regions are more luminous than those farther out in radius. Both galaxies are more distant than most of those observed by Kennicutt et al., and resolution differences may impact our results.